NASA/TP—2008-214953

Application of Ruze Equation for Inflatable Aperture Antennas

Bryan W. Welch
Glenn Research Center, Cleveland, Ohio

April 2008

NASA STI Program . . . in Profile

Since its founding, NASA has been dedicated to the advancement of aeronautics and space science. The NASA Scientific and Technical Information (STI) program plays a key part in helping NASA maintain this important role.

The NASA STI Program operates under the auspices of the Agency Chief Information Officer. It collects, organizes, provides for archiving, and disseminates NASA's STI. The NASA STI program provides access to the NASA Aeronautics and Space Database and its public interface, the NASA Technical Reports Server, thus providing one of the largest collections of aeronautical and space science STI in the world. Results are published in both non-NASA channels and by NASA in the NASA STI Report Series, which includes the following report types:

- TECHNICAL PUBLICATION. Reports of completed research or a major significant phase of research that present the results of NASA programs and include extensive data or theoretical analysis. Includes compilations of significant scientific and technical data and information deemed to be of continuing reference value. NASA counterpart of peer-reviewed formal professional papers but has less stringent limitations on manuscript length and extent of graphic presentations.

- TECHNICAL MEMORANDUM. Scientific and technical findings that are preliminary or of specialized interest, e.g., quick release reports, working papers, and bibliographies that contain minimal annotation. Does not contain extensive analysis.

- CONTRACTOR REPORT. Scientific and technical findings by NASA-sponsored contractors and grantees.

- CONFERENCE PUBLICATION. Collected papers from scientific and technical conferences, symposia, seminars, or other meetings sponsored or cosponsored by NASA.

- SPECIAL PUBLICATION. Scientific, technical, or historical information from NASA programs, projects, and missions, often concerned with subjects having substantial public interest.

- TECHNICAL TRANSLATION. English-language translations of foreign scientific and technical material pertinent to NASA's mission.

Specialized services also include creating custom thesauri, building customized databases, organizing and publishing research results.

For more information about the NASA STI program, see the following:

- Access the NASA STI program home page at *http://www.sti.nasa.gov*

- E-mail your question via the Internet to *help@sti.nasa.gov*

- Fax your question to the NASA STI Help Desk at 301–621–0134

- Telephone the NASA STI Help Desk at 301–621–0390

- Write to:
  NASA Center for AeroSpace Information (CASI)
  7115 Standard Drive
  Hanover, MD 21076–1320

NASA/TP—2008-214953

Application of Ruze Equation for Inflatable Aperture Antennas

Bryan W. Welch
Glenn Research Center, Cleveland, Ohio

National Aeronautics and
Space Administration

Glenn Research Center
Cleveland, Ohio 44135

April 2008

Acknowledgments

I wish to thank my mentor and colleague, Dr. Robert Romanofsky, for encouraging me to perform this study; Dr. Murad Hizlan for giving support and clarity during the pursuit of my Master's Degree; and NASA Glenn Research Center for providing me the opportunity to pursue my master's degree.

This report contains preliminary findings, subject to revision as analysis proceeds.

Level of Review: This material has been technically reviewed by an expert single reviewer.

Available from

NASA Center for Aerospace Information
7115 Standard Drive
Hanover, MD 21076–1320

National Technical Information Service
5285 Port Royal Road
Springfield, VA 22161

Available electronically at http://gltrs.grc.nasa.gov

Application of Ruze Equation for Inflatable Aperture Antennas

Bryan W. Welch
National Aeronautics and Space Administration
Glenn Research Center
Cleveland, Ohio 44135

Summary

Inflatable aperture reflector antennas are an emerging technology that NASA is investigating for potential uses in science and exploration missions. As inflatable aperture antennas have not been proven fully qualified for space missions, they must be characterized properly so that the behavior of the antennas can be known in advance. To properly characterize the inflatable aperture antenna, testing must be performed in a relevant environment, such as a vacuum chamber. Since the capability of having a radiofrequency (RF) test facility inside a vacuum chamber did not exist at NASA Glenn Research Center, a different methodology had to be utilized.

The proposal to test an inflatable aperture antenna in a vacuum chamber entailed performing a photogrammetry study of the antenna surface by using laser ranging measurements. A root-mean-square (rms) error term was derived from the photogrammetry study to calculate the antenna surface loss as described by the Ruze equation. However, initial testing showed that problems existed in using the Ruze equation to calculate the loss due to errors on the antenna surface.

This study utilized RF measurements obtained in a near-field antenna range and photogrammetry data taken from a laser range scanner to compare the expected performance of the test antenna (via the Ruze equation) with the actual RF patterns and directivity measurements. Results showed that the Ruze equation overstated the degradation in the directivity calculation. Therefore, when the photogrammetry study is performed on the test antennas in the vacuum chamber, a more complex equation must be used in light of the fact that the Ruze theory overstates the loss in directivity for inflatable aperture reflector antennas.

Introduction

The intention of this study was to determine whether or not the Ruze equation for the degradation in directivity was appropriate for evaluating the directivity performance of inflatable aperture antennas. When evaluating the performance of these antennas, testing must be performed in an appropriate environment before an antenna can be considered for use on a space mission. The methodology would be to place the inflatable antenna in a thermal vacuum chamber to analyze thermal distortions from simulated full Sun to total eclipse. The testing must be conducted in a thermal vacuum chamber and not in a standard anechoic chamber. The reason is that the inflatable antenna will undergo changes in its paraboloidal shape as a result of the effects from the coefficient of thermal expansion and solar flux variation experienced in the space environment, where the changes occur on time scales on the order of minutes.

One limitation of the proposed testing methodology was that the thermal vacuum chamber did not contain any near-field or far-field testing chambers. However, since the thermal vacuum chamber did have windows, it was possible to perform a photogrammetry analysis of the surface of the inflatable antenna. After the photogrammetry analysis was completed, a root-mean-square (rms) surface error was computed by utilizing the Ruze equation. From the Ruze equation, the test provided information only on the loss in directivity.

Intended Purpose of Work

The present study was conducted to examine the viability of using the Ruze equation when evaluating inflatable aperture antennas. The Ruze equation utilizes information on the rms surface error of an antenna and the wavelength at which the antenna will be operating to determine the loss in directivity due to surface errors (ref. 1). Commonly, the surface errors that exist on an antenna are thought of as phase errors. Geometrical optics states that rays originating from the feed of an antenna, placed at the focal point of the paraboloid, will travel to the antenna surface and reflect in the axial direction such that the rays are parallel to each other at the aperture plane. Once these rays reach the aperture plane, they will have all traveled the same distance and the aperture will be a plane of constant phase (ref. 2).

However, when surface errors exist, there can be a change in the direction that the reflected ray will travel, which can also change the phase of the ray when the ray reaches the aperture plane. Snell's law states that the incident and reflection angles from the surface normal will be equal (ref. 2). Surface errors will cause a change in the direction that the surface normal vector will be pointing and therefore will change the direction that the reflected ray will travel. In perfect paraboloid antennas, the surface normal can be easily determined from the equation of the paraboloid. However, when the antenna no longer maintains the perfect paraboloidal shape, the surface normal vector direction will be modified from the ideal surface normal vector. If the errors in the antenna surface are such that the incident angle on the antenna surface is decreased from the ideal incident angle, the

reflecting rays will be propagated in a direction that is not parallel to the axial direction. The reflected rays will thus have a smaller radial distance from the feed in the aperture plane. On the other hand, if the errors in the antenna surface are such that the incident angle on the antenna surface is increased from the ideal incident angle, the reflection rays will have a larger radial distance from the feed in the aperture plane. The changes in the direction of the reflected rays will also cause a change in distance that the reflected ray must be propagated. Phase errors are also introduced because of this reflection angle error.

The above effect is what creates errors in the phase front on the aperture plane. Rays will not travel in the appropriate direction, which is parallel to the axial direction of the antenna. The distance that the rays travel will be modified and the phase of the particular ray will be in error. The Ruze equation attempts to characterize these effects and determine the degradation of the directivity of the antenna based on the rms surface error and the wavelength at which the antenna is operating.

The methodology of this study consisted of performing a radiofrequency (RF) scan in a near-field antenna testing range to determine the directivity and beam patterns of an offset inflatable aperture antenna. Concurrently, laser ranging scans were performed to determine the rms surface error to be used in the Ruze equation. Both these tests were performed on the inflatable aperture antenna while under multiple pressurizations, from which cases where wrinkling occurred and cases where over-inflation existed could be examined. Directivity measurements from the radiofrequency scan were compared with the predicted directivity with known inefficiencies of the antenna. This comparison determined the additional loss that existed as a result of the surface errors of the inflatable antenna. The Ruze equation was utilized to determine the predicted surface error loss. The next step was to compare the differences between the radiofrequency-scan-derived surface error loss and the surface error loss that the Ruze equation predicted. This study was to determine if these types of errors would be a factor in prohibiting the Ruze equation from being an accurate procedure for ascertaining the loss in directivity for inflatable aperture antennas.

Ruze Equation

The Ruze equation makes assumptions about the nature of the surface errors: that is, that (a) the surface errors are random in nature and are uncorrelated with each other (ref. 1) and (b) the errors on the antenna surface are of the nature of a Gaussian probability density function. Inflatable aperture antennas have more than random surface errors present on the antenna surface. These errors are called the *W*-curve errors and create a nonparaboloidal shape at the edges of the antenna surface and a spherical aberration near the vertex (ref. 3). This causes many errors to be created near the edge of the antenna. The *W*-curve errors also create a change in the shape of the paraboloidal portion of the inflatable antenna, which can be characterized as the focal point of the paraboloid no longer being at the same location as the feed of the antenna. Other errors that can exist on an inflatable antenna include those resulting from improper inflation: overinflation can cause a change in the ideal focal point of the paraboloid, or underinflation can cause wrinkles to form on the antenna surface, creating additional surface errors.

Symbols

A	Ruze loss correction factor
a	radius of antenna
c	radius of one of the N correlation regions of antenna aperture
D	diameter of antenna
e	continuous error between actual and ideal antenna surfaces
f	focal length for paraboloid
f/D	ratio of focal length to diameter of antenna
$f(r,\phi)$	in-phase illumination function in terms of aperture coordinates
G	axial gain of antenna
G_0	axial gain of antenna without phase error
L_R	loss in directivity due to surface errors
L_x	length of antenna in x-axis
L_y	length of antenna in y-axis
M	number of discrete antenna surface points
N	regions of antenna aperture
N_M	minimum number of sampling points
N_x	minimum number of sampling points in x-dimension
N_y	minimum number of sampling points in y-dimension
$\overline{P}$	power sum
r	radial distance variable for antenna
r,ϕ	aperture coordinates
S	area of antenna surface
x,y	antenna coordinates from which error is measured
x,y,z	Cartesian coordinates along paraboloid
Δz_i	deterministic error between the actual and ideal antenna surface
$\overline{\delta}$	illumination weighted mean-square phase error
$\overline{\delta}^2$	weighted mean-square phase error, $\eta(\pi D/\lambda)^2$
δ_N^2	variance of phase error
$\delta(r,\phi)$	phase error in terms of aperture coordinates
ε	rms surface error of antenna
η	known efficiency of antenna

θ,ϕ	far-field coordinates
$\Lambda_1( )$	Lambda function
λ	wavelength at which antenna is operating
ξ_i	random measuring equipment-induced error
σ	standard deviation of measuring equipment error

Background

This section gives detailed information on inflatable antennas, including their benefits and limitations, and illustrations of surface errors and their effect on the aperture phase front; the Ruze equation and theory; the calculation of the rms surface errors; and the Nyquist surface sampling requirements for an appropriate photogrammetry study, which is derived from requirements of the Nyquist sampling theorem.

Inflatable Aperture Antennas

Inflatable aperture antennas are an emerging research technology and provide several advantages over standard reflector antenna systems. Inflatable aperture antennas can provide benefits in terms of size and density and are capable of being packed in a small stowage space and inflated to full size at a later time (ref. 4). They are designed to be inflated to the designed paraboloidal shape, which would be held in place by some form of structural supports. However, these antennas need an inflation system present, which is not necessary for standard parabolic reflector antennas. The aerial density of inflatable aperture antennas that have been developed has been lower than 1 kg/m^2 (ref. 4).

The only inflatable aperture antenna flown in space to date was the 14-m Inflatable Antenna Experiment (IAE) that was launched aboard the Space Shuttle Endeavor (Mission STS−77) in 1996. Figure 1 shows an image of the IAE as viewed from the shuttle (ref. 4).

The IAE lasted 90 min, during which the antenna support structure was successfully deployed to the proper shape. However, the lens-shaped reflector failed to inflate, which meant that no in-flight measurements regarding the surface accuracy of the antenna were obtained (ref. 4).

Several inflatable aperture antennas have been under investigation at NASA Glenn Research Center since 2004. The Center has been partnering with SRS Technologies, which has manufactured several inflatable aperture antennas, including a 0.3-m offset inflatable antenna (refs. 4 to 8) and a 4- by 6-m offset inflatable antenna (ref. 4). The 0.3-m offset inflatable antenna, shown in figure 2, was tested at 8.4 GHz. The performance of the antenna was comparable to that of a conventional rigid reflector antenna of a similar size. It also performed well compared with the theoretical predictions (refs. 4 to 8).

A 4- by 6-m offset inflatable antenna manufactured by SRS Technologies is inflated in the aperture and in the torus, which is used to support the aperture. This antenna, shown inside the NASA Glenn Research Center near-field test facility (fig. 3), was tested and characterized at 8.4 and 32 GHz (ref. 4). Measured directivities were 49.4 and 51.6 dBi, which corresponded to efficiencies of 71 percent at 8.4 GHz and 8 percent at 32 GHz (ref. 4). The rms surface error was measured for this antenna and was computed to be 3.5 mm. According to the Ruze equation, this amount of surface error would lead to much greater gain degradation at the Ka-band frequency of 32 GHz (i.e., 99 dB). Phase plots of the near-field data show macroscopic surface errors, which contribute to the gain degradation, and also reveal that some of the surface errors are not independent of each other.

Figure 1.—Inflatable antenna experiment.

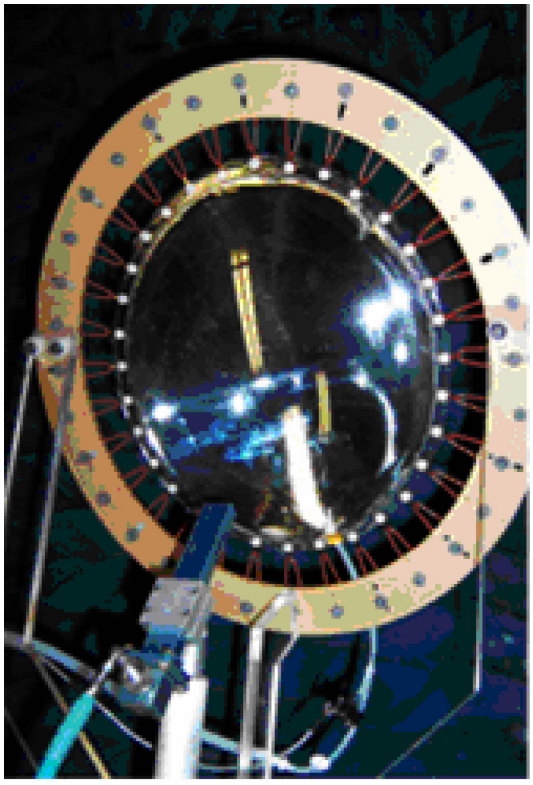

Figure 2.—0.3-m offset inflatable antenna.

Figure 3.—4- by 6-m offset inflatable antenna.

One of the main limitations of the inflatable aperture antennas under much investigation is their inability to overcome the non-ideal paraboloidal shape known as the Hencky curve, or the *W*-curve. The Hencky curve is an attribute of inflatable structures involving the amount of strain on the surface of the walls of the structure, producing an ill-shaped paraboloid (ref. 3). The ill-shaped paraboloid creates what is called spherical aberration in the reflected fields. The Hencky curve prevents an inflatable structure from achieving a paraboloidal shape. The result of the Hencky curve is that the boundary edge of the reflector will be spread out in comparison with the configuration of an ideal paraboloid. This phenomenon is illustrated in the plot of figure 4 (ref. 3), in which *a* is the radius of the antenna and *r* is the radial distance variable for the antenna.

As figure 4 shows, the only locations of an ideal surface may be located at the vertex, or at the edge boundary of the antenna, shown at the left and right sides of the plot. The effect of the Hencky curve is that the antenna begins to become too steep too early with regard to its slope away from the vertex. As the membrane structure reaches the edge boundary, the surface spreads out until the boundary is reached. Another way to understand the effects of the Hencky curve is to recognize that the design focal point will no longer be at the location of the ideal focal point. Techniques to control this effect have been somewhat effective. These techniques include fabricating the inflatable aperture reflectors with electroactive polymers (ref. 3) and placing structures around the edge boundary of the reflector to help control the shape more accurately (refs. 9 and 10).

Ruze Theory

The surface errors that exist on an antenna are thought of as phase errors because surface errors cause the phase front at the aperture plane to fluctuate. An example of an ideal paraboloidal antenna surface reflection ray is illustrated in figure 5. For an antenna operating in transmit mode, geometric optics states that rays originating from the feed of an antenna travel to the antenna surface and are reflected traveling parallel to the axial direction of the antenna. All the rays are thought of as being parallel when one is dealing with an ideal paraboloidal surface. Once these rays reach the aperture plane, they will have traveled the same distance and the aperture would be a plane of constant phase (ref. 3).

In figure 5, the dashed line shows the ray that originates from the feed at the focal point location and travels to the antenna surface. The antenna surface, the solid line, is that of an ideal paraboloid. The dotted line denotes the normal vector at the point of reflection on the antenna surface. Finally, the dashed-dotted line illustrates the ray reflecting off the antenna surface and traveling parallel to the axial direction, defined as the *x*-axis of the plot.

However, when surface errors exist, there can be a change in the direction that the reflected ray will travel, and this change can also alter the phase of the ray when the ray reaches the aperture plane. Snell's law states that the incident and reflection angles from the surface normal will be equal (ref. 3). Surface errors will cause a change in the direction that the surface normal vector will be pointing and therefore change the direction that the reflected ray will travel. The plot in figure 6 illustrates this effect for a non-ideal paraboloidal surface. Despite the type of surface errors that exist, Snell's law must be true. Thus, even when the antenna no longer maintains the perfect paraboloidal shape, the incident and reflection angles from the surface normal must still be equal. The result is that the reflected rays will no longer travel in the direction parallel to the axial direction of the antenna. The changes in the direction of the reflecting rays will also cause a change in the distance that the reflecting ray must be propagated; consequently, phase errors are also introduced because this reflection angle error deviates from the ideal.

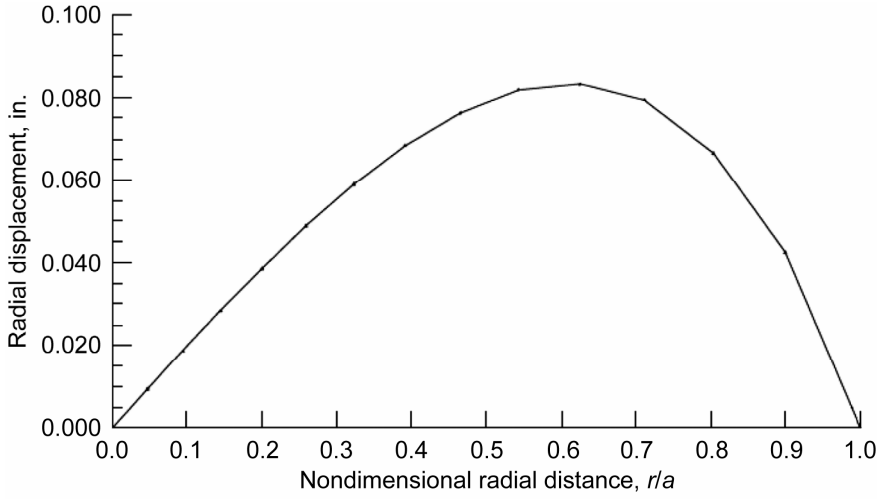

Figure 4.—Hencky curve error.

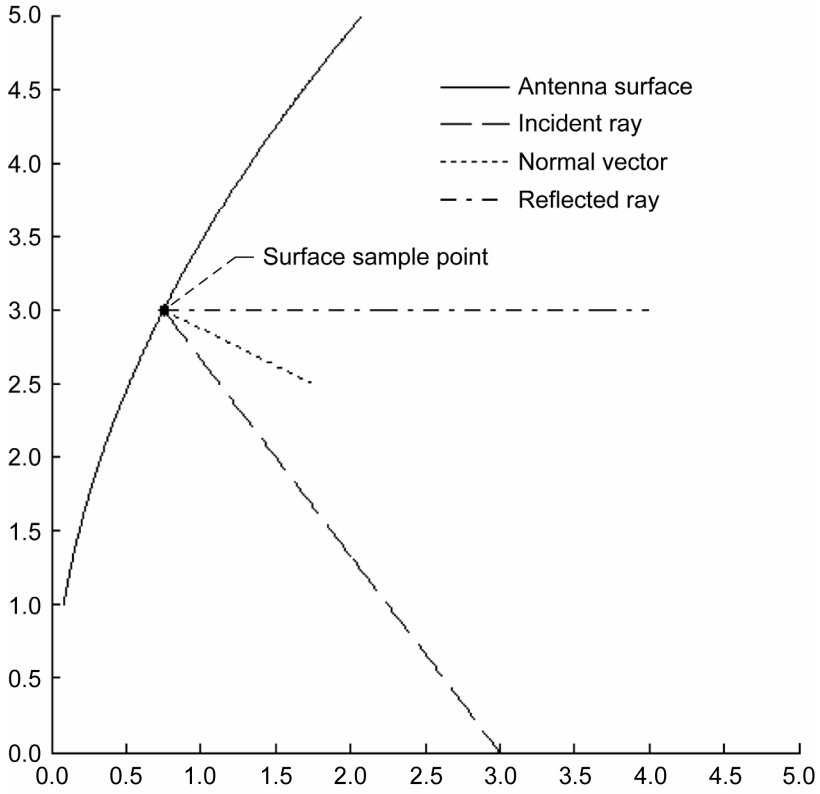

Figure 5.—Ideal paraboloidal antenna surface reflection.

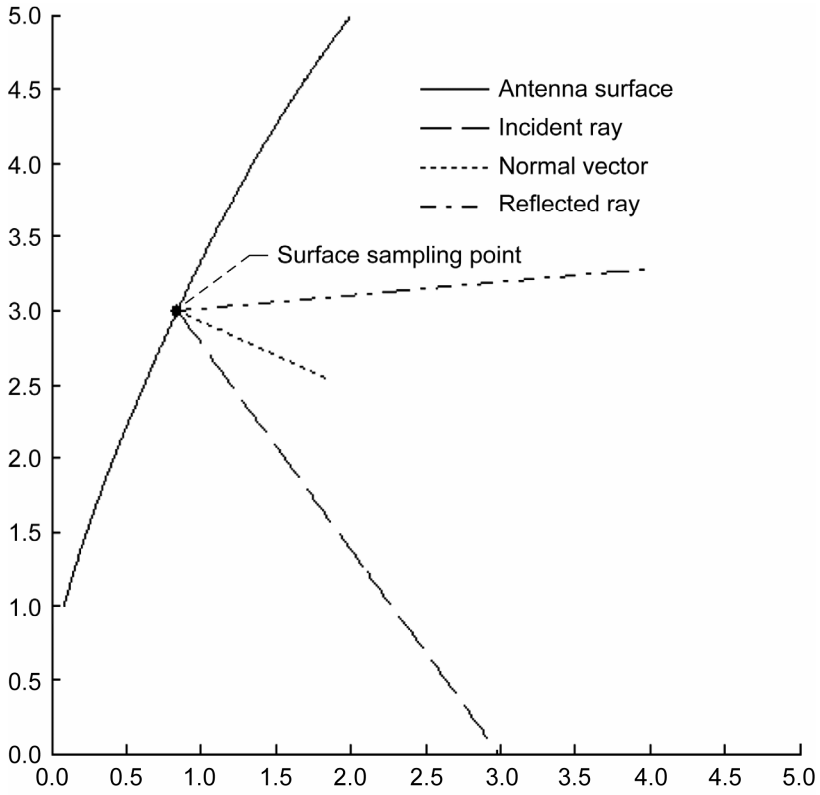

Figure 6.—Non-ideal paraboloidal antenna surface reflection.

In figure 6, the line types have the same meaning as in figure 5 with regard to antenna surface, incident ray, normal vector, and reflected ray. The exception is that the solid line in figure 6 is the corrupted antenna surface, and the reflected ray is traveling in the non-ideal direction as compared with the direction in which it would travel in the ideal paraboloidal case. This aforementioned effect is what creates errors in the phase front on the aperture plane. Rays do not travel in the appropriate direction, which is parallel to the axial direction of the antenna. The distance that the rays travel will be modified and the phase of the particular ray will be in error.

The Ruze equation attempts to understand these effects and determine the degradation of the antenna directivity based on the surface rms value and the wavelength at which the antenna is operating (ref. 1). The derivation of the Ruze equation can be found in reference 1. The equation was derived from a first principles methodology. Ruze states that the axial gain of a circular antenna with a phase error can be defined as

$$G = \frac{4\pi}{\lambda^2} \frac{\left| \int_0^{2\pi} \int_0^a f(r,\phi) e^{j\delta(r,\phi)} r dr d\phi \right|^2}{\int_0^{2\pi} \int_0^a f^2(r,\phi) r dr d\phi} \tag{1}$$

where

G	axial gain of antenna
$f(r,\phi)$	in-phase illumination function in terms of aperture coordinates
r,ϕ	aperture coordinates
$\delta(r,\phi)$	phase error in terms of aperture coordinates
λ	wavelength at which antenna is operating

Making the assumption that the phase errors are small, the exponential in the numerator of equation (1) can be expanded into a power series. When the ratio of the gain, with errors, is taken to the gain with zero errors, it can be approximated as

$$\frac{G}{G_0} \approx 1 - \overline{\delta}^2 + \overline{\delta}^2 \tag{2}$$

where

G_0	axial gain of antenna without phase error $\eta(\pi D/\lambda)^2$
D	diameter of antenna
$\overline{\delta}^2$	weighted mean-square phase error
$\overline{\delta}$	illumination weighted mean-square phase error
η	known efficiency of antenna

The mean-square phase error and illumination weighted mean-square phase error are defined by equations (3) and (4), respectively:

$$\overline{\delta^2} = \frac{\int_0^{2\pi} \int_0^a f(r,\phi) \delta^2(r,\phi) r dr d\phi}{\int_0^{2\pi} \int_0^a f(r,\phi) r dr d\phi} \tag{3}$$

$$\overline{\delta} = \frac{\int_0^{2\pi} \int_0^a f(r,\phi) \delta(r,\phi) r dr d\phi}{\int_0^{2\pi} \int_0^a f(r,\phi) r dr d\phi} \tag{4}$$

Note that the difference between the terms in equations (3) and (4) is that the phase error term used in the numerator of equation (3) is squared, whereas the term is to the power of 1 in equation (4). If the phase reference plane is chosen such that $\overline{\delta}$, the illumination weighted mean-square phase error, is set to 0, then equation (2) reduces to

$$\frac{G}{G_0} \approx 1 - \overline{\delta}_0^2 \tag{5}$$

The relationship provided in equation (5) shows that the loss in gain due to phase errors is equal to the weighted mean-square phase error. This relationship is valid for any type of surface error pattern present on any antenna. The next step that Ruze took in the development of his equation was to extend the previous equation for the case of large phase errors. Ruze did not have detailed knowledge of the phase front error, so he had to utilize the statistical properties of the surface error.

Ruze began his advanced analysis by separating the aperture into N regions. Each region (which he called a "hatbox" because of the constant amplitude over the circular region) has a phase error and is not related to any neighboring regions. The axial field can be assumed to be the sum of the individual contributions from all the N regions, as illustrated in figure 7, in which c is the radius of one of the N correlation regions.

If there are N unit field vectors with a zero phase error, then the power sum can be derived as N^2. However, since there are phase errors, if it is assumed that the phase errors are Gaussian in nature with a variance $\overline{\delta}^2$ in radians, then the power sum can be expressed as

$$\overline{P} = N^2 e^{-\overline{\delta}_N^2} + N\left(1 - e^{-\overline{\delta}_N^2}\right) \tag{6}$$

where $\overline{P}$ is the power sum and $\overline{\delta}_N^2$ is the variance of the phase error.

The expected radiation pattern of the model shown in figure 7 can also be derived. First, it must be assumed that the phase values are correlated in a diameter of $2c$, which is the

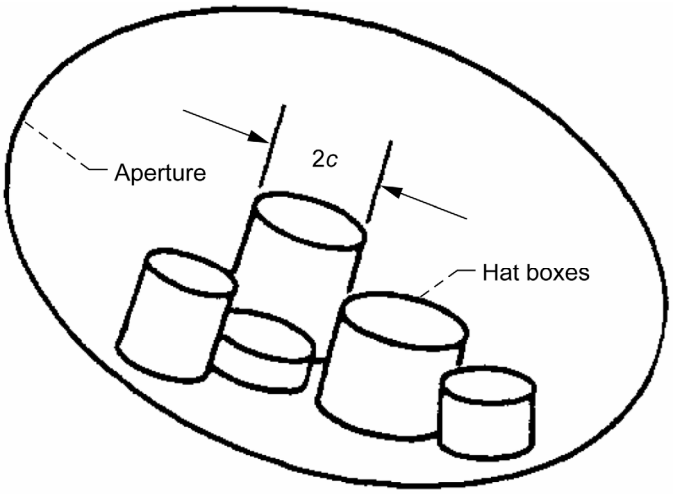

Figure 7.—Aperture divided into *N* hatbox regions. Radius, *c*.

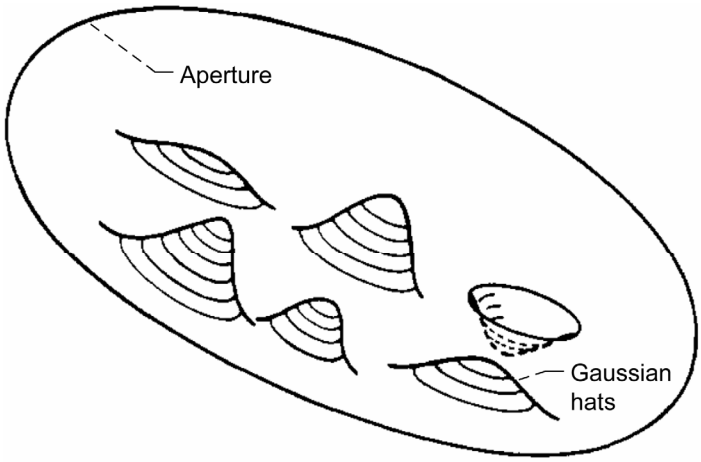

Figure 8.—Aperture divided into *N* hat regions.

diameter of the regions known as hatboxes (fig. 7). Phase values are uncorrelated for distances larger than 2*c*. Also, as before, the phase errors have a Gaussian distribution with a variance $\overline{\delta}_N^2$ in radians. Finally, the number of regions must be large enough to satisfy the following relationship:

$$N = \left(\frac{D}{2c}\right)^2 >> 1 \tag{7}$$

From these assumptions, the expected radiation pattern in the far-field can be derived as

$$G(\theta,\phi) = G_0(\theta,\phi)e^{-\overline{\delta}_N^2} + \left(\frac{2\pi c}{\lambda}\right)^2 \left(1 - e^{-\overline{\delta}_N^2}\right) \Lambda_1\left(\frac{2\pi c \sin\theta}{\lambda}\right) \tag{8}$$

where θ and ϕ are the far-field coordinates and $\Lambda_1(\ )$ is the Lambda function.

Equation (8) shows a similarity to equation (6) in that the zero-error radiation diagram is reduced by an exponential term. Also added is a scattered field that has a beam width that is inversely proportional to the radius of the correlated regions. Equation (8) can be improved if the hatboxes shown in figure 7 are replaced with the "hats" shown in figure 8.

If the phase front errors are assumed to have a Gaussian shape, the expected radiation pattern can be evaluated and defined as

$$G(\theta,\phi) = G_0(\theta,\phi)e^{-\overline{\delta}_N^2} + \left(\frac{2\pi c}{\lambda}\right)^2 e^{-\overline{\delta}_N^2} \sum_{n=1}^{\infty} \frac{\overline{\delta}_N^{2n}}{n \cdot n!} e^{-(\pi c \sin\theta/\lambda)^2/n} \tag{9}$$

Equation (9) can be modified to express the reduction in the axial gain:

$$\frac{G}{G_0} = e^{-\bar{\delta}_N^2} + \frac{1}{\eta}\left(\frac{2c}{D}\right)^2 e^{-\bar{\delta}_N^2} \sum_{n=1}^{\infty} \frac{\bar{\delta}_N^{2n}}{n \cdot n!} \tag{10}$$

For correlation regions that are small compared with the antenna diameter, the second term of equation (10) can be ignored to produce

$$G = \eta\left(\frac{\pi D}{\lambda}\right)^2 e^{-\left(\frac{4\pi\varepsilon}{\lambda}\right)^2} \tag{11}$$

where ε is the rms surface error of the antenna.

Since the directivity of an antenna with zero error is known as $\eta(\pi D/\lambda)^2$, the loss due to surface errors can be represented as the Ruze equation:

$$L_R = e^{-(4\pi\varepsilon/\lambda)^2} \tag{12}$$

where L_R is the loss in directivity due to surface errors.

Ruze found through experimentation that the surface error directivity loss was too large by a factor of A (ref. 1). This factor was determined by the procedure in which the surface errors were computed and the depth of the antenna was defined. Surface errors can be calculated from axial errors or normal errors. The depth of the antenna is defined by the ratio of the focal length to the diameter of the antenna f/D. The curves that define the term A are shown in figure 9 (ref. 1). The modified Ruze equation is

$$L_R = e^{-A(4\pi\varepsilon/\lambda)^2} \tag{13}$$

where A is the Ruze loss correction factor.

The final topic in the discussion of the Ruze theory is the limitations of the Ruze equation. The limitations are based on assumptions that were made during the derivation of the statistical estimates of the phase errors that are present for the antenna. Five distinct assumptions are noted by Ruze (ref. 1):

(1) The surface errors on the antenna are random in nature.
(2) The surface errors are uniformly distributed over the aperture.
(3) The surface errors are distributed in fixed, circular correlation regions.
(4) The aperture of the antenna is much larger compared with the diameter correlation region, $D >> 2c$.
(5) The surface errors have a Gaussian spatial phase correlation.

The supposed limitations of the Ruze equation regarding its usage for inflatable aperture antennas can be looked at with respect to the above assumptions. First, surface errors on these antennas originate from the errors associated with the Hencky curve and result from wrinkles caused by improper inflation of the aperture. Second, the surface errors of the antennas may not be uniformly distributed over the aperture because of the location where wrinkles typically occur. Finally, the surface errors are not distributed in fixed, circular correlation regions by reason of the nature of the errors associated with the Hencky profile. It can be established from these conclusions that the Ruze equation may not be applicable to inflatable aperture antennas.

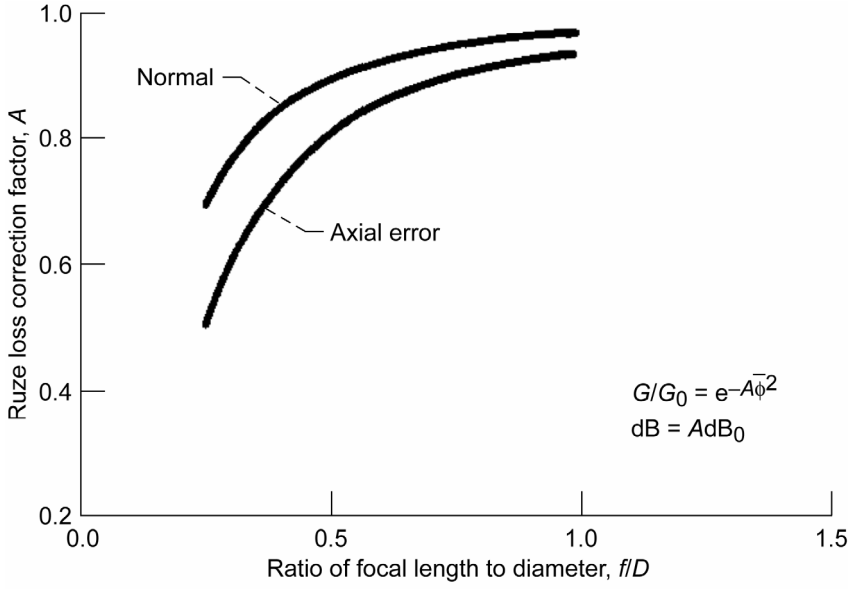

Figure 9.—Ruze loss correction factor, A.

Root-Mean-Square Error Calculation

The accuracy of a surface compared with an ideal version of the surface can be computed via the RMS of the surface error. The rms of the surface error is a parameter that is used in the Ruze equation to compute the predicted loss in directivity due to errors on the antenna surface. The most accurate rms error is computed from the error between continuous functions of the actual and ideal antenna surfaces (ref. 11):

$$\varepsilon = \sqrt{\frac{1}{S}\int\int_{S} e^2(x,y)dxdy} \tag{14}$$

where S is the area of the antenna surface; e is the continuous error between actual and ideal antenna surfaces; and x and y are the antenna coordinates from which the error is measured.

It is important to note that ε is not the square root of a variance but rather is a deterministic quantity originating from the error from the actual shape of an antenna. Equation (14) assumes that the actual surface is known in the form of a continuous function. Since the actual surface is not known in the form of a continuous function, but rather from a discrete set of data points, the measurement error also must be taken into account. Equation (15) is an approximation of the continuous rms surface error for M discrete points measured on the antenna surface and also takes into account the measuring device error (ref. 11):

$$\varepsilon = \sqrt{\frac{1}{M}\sum_{i=1}^{M}\left(\xi_i + \Delta z_i\right)^2} \tag{15}$$

where M is the number of discrete antenna surface points; ξ_i is the random measuring equipment-induced error; and Δz_i is the deterministic error between the actual and ideal antenna surface.

However, when $\varepsilon >> \sigma$, where σ is the standard deviation of the measuring equipment error, the dominant term of the error is the deterministic error between the actual and ideal antenna surfaces. Therefore, the random measuring equipment induced error can be neglected, as such, in equation (16), which is used later to compute rms surface accuracies:

$$\varepsilon = \sqrt{\frac{1}{M}\sum_{i=1}^{M}\left(\Delta z_i\right)^2} \tag{16}$$

Antenna Surface Sampling Requirements

Surface sampling of discrete antenna points is dictated by the Nyquist sampling rate. The Nyquist sampling theorem requires that a function have a spectrum that exists and is nonvanishing over the finite region of wave-number space (ref. 12). Under the completion of these two requirements, the function may be exactly reproduced when the function is sampled on a periodic grid at a rate of at least two times the maximum frequency. The minimum number of points necessary in a single dimension can be derived in equation (17) for the x-dimension and in equation (18) for the y-dimension, assuming that the data will be analyzed over the z-dimension:

$$N_x = \left\lfloor \frac{2L_x}{\lambda} \right\rfloor + 1 \tag{17}$$

$$N_y = \left\lfloor \frac{2L_y}{\lambda} \right\rfloor + 1 \tag{18}$$

where

N_x	minimum number of sampling points in x-dimension
L_x	length of antenna in x-axis
N_y	minimum number of sampling points in y-dimension
L_y	length of antenna in y-axis
$\lfloor\ \rfloor$	floor function

If the antenna aperture were rectangular in nature, then the minimum number of sampling points over the antenna surface would be N_xN_y. However, since the inflatable aperture antenna is circular, the minimum number of sampling points in the x-dimension is equal to the minimum number of sampling points in the y-dimension. Therefore, the total minimum number of sampling points is the area of the antenna divided by the area of a sampling point and is defined by

$$N_M = \left\lfloor \frac{\pi D^2}{\lambda^2} \right\rfloor + 1 \tag{19}$$

where N_M is the minimum number of sampling points.

The minimum number of sampling points over the aperture is defined by equation (19). However, there may be cases in which it is necessary to oversample the antenna surface, such as when there are known wrinkles that have a high spatial frequency or when there is a desire to examine microscopic surface errors. A limitation that may exist for inflatable aperture antennas is a nonconstant antenna surface over the duration of the scanning period. If this is the case, the number of sampling points should be kept near the Nyquist sampling minimum.

Equipment and Methodology

This section documents the various testing instruments and analysis routines that were utilized in the analysis for this study. Four subsections provide information on (a) the 0.3-m offset inflatable aperture antenna; (b) the near-field RF

scanning equipment; (c) the equipment used to perform the photogrammetry study, along with the known errors; and (d) the Matlab software routine used to transform the photogrammetry data to an appropriate coordinate system for use in calculating the rms surface error.

Offset Inflatable Reflector Antenna Specifications

The antenna that was under testing in this study was a 0.3-m offset inflatable aperture reflector antenna. It was manufactured by SRS Technologies and underwent various tests at NASA Glenn Research Center in 2004 (ref. 6). For the purpose of creating various levels of surface errors, the antenna was tested at various pressurization levels: 0.00, 0.03, 0.04, 0.05, 0.06, and 0.07 in. H_2O of ambient air. An illustration of the 0.3-m offset inflatable aperture antenna being installed in the far-field test facility from 2004 is shown in figure 10.

The antenna was tested at 8.4 GHz with a feed installed that utilized an 11-dB taper, creating a known efficiency of 0.68. Parameters of the geometry of the antenna are listed in table I (ref. 6).

The side profile of the antenna is shown in figure 11, and a schematic of its design with the support structure is presented in figure 12.

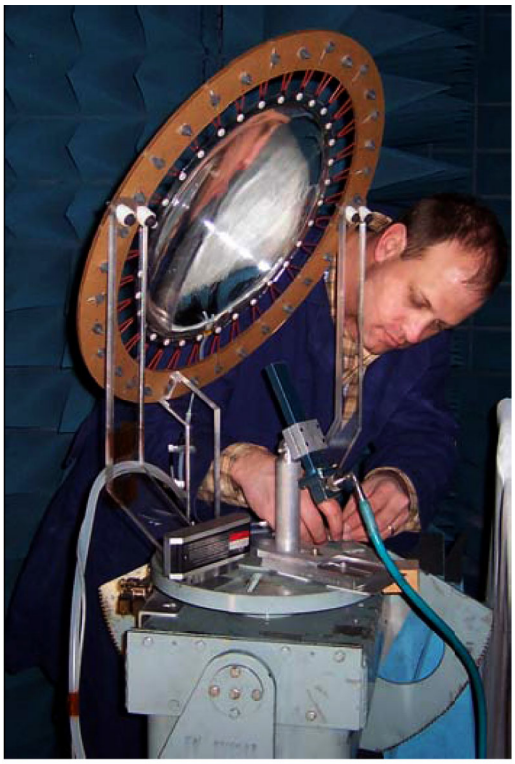

Figure 10.—Installation of 0.3-m offset inflatable aperture antenna.

Planar Near-Field Antenna Test Facility

NASA Glenn Research Center operates a planar near-field antenna test facility that has capabilities of measuring the electromagnetic radiation characteristics of antenna systems and components to support the development of advanced antenna technologies for commercial communications systems and NASA missions. A photograph of the planar near-field antenna test facility is presented in figure 13, and the facility properties are listed in table II.

The planar near-field antenna test facility was utilized to measure the electromagnetic fields of the 0.3-m offset inflatable aperture antenna at a frequency of 8.4 GHz. Vertical and horizontal polarization measurements were taken to compute the co-polarization and cross-polarization fields. Measurements were taken under all six antenna inflation pressurizations. Figure 14 presents an image of the 0.3-m offset inflatable aperture antenna on the pedestal of the planar near-field antenna test facility prior to testing.

Leica 200 Photogrammetry System

The Leica 200 photogrammetry system was utilized to perform a photogrammetry study of the surface of the 0.3-m inflatable aperture antenna. The Leica 200 utilizes laser ranging measurements with known pointing angles to determine the location of the object being measured. Figure 15 is a photograph of the Leica 200 photogrammetry system in the planar near-field antenna test facility.

The Leica 200 photogrammetry system has an expected error on the order of ±25 μm. However, there are occasions where false measurements are made. To deal with this issue, the Leica 200 photogrammetry system includes a software

TABLE I.—0.3-m OFFSET INFLATABLE APERTURE ANTENNA GEOMETRIC PROPERTIES
[See fig. 11 for geometry.]

Diameter, D, m	0.3048
Wavelength, λ, m at 8.4 GHz	0.0357
Focal length, f, m	0.152
Focal length/diameter, f/D	0.50
Offset distance, cm	2.54
Depth, cm	3.8
Major length, m	0.353
Angle, deg	
Tilt	52.05
Half-cone	42.53
Slope	59.74

TABLE II.—PROPERTIES OF PLANAR NEAR-FIELD ANTENNA TEST FACILITY

Frequency range, GHz	1 to 40
Scanning plane, ft	22 by 22
Positioning and alignment method	Laser
Dynamic range, dB	80
Antenna diameter, ft	Up to 15
Scanning plane flatness, in. rms	0.004

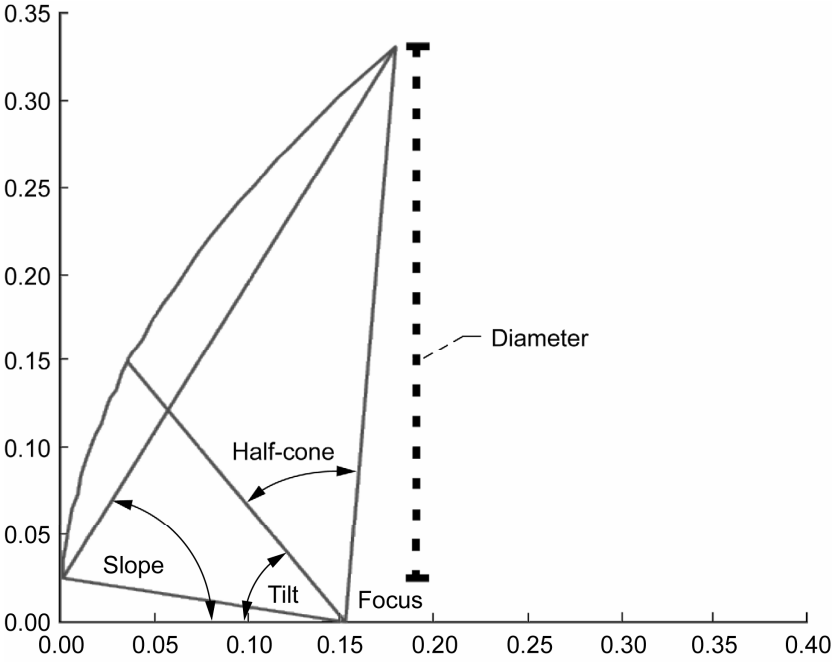

Figure 11.—Profile geometry of 0.3-m antenna.

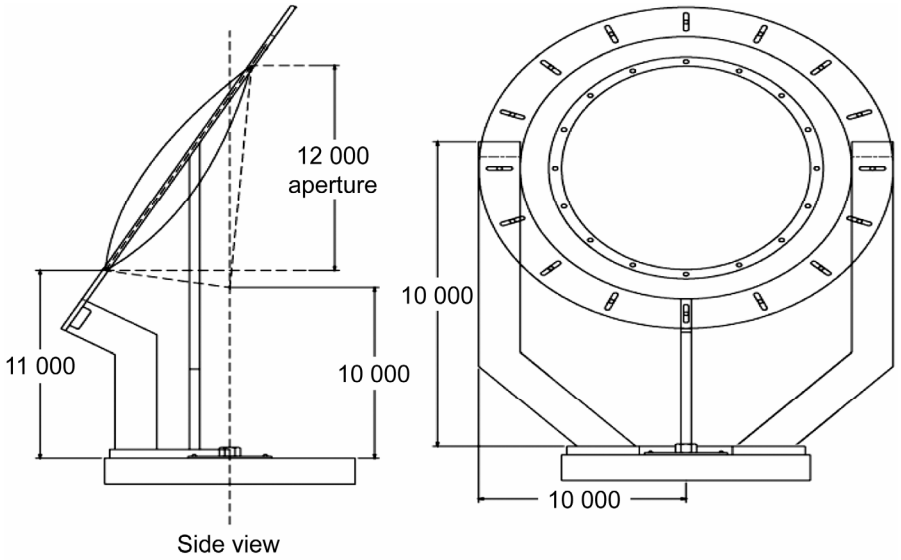

Figure 12.—Design and support structure of 0.3-m antenna.

Figure 13.—Planar near-field antenna test facility.

Figure 14.—The 0.3-m antenna in planar near-field antenna test facility.

Figure 15.—Leica 200 photogrammetry system.

package called CloudViewer, which allows the user to view the measured points and delete erroneous data points. Sampling distance is an input to the laser ranging metrology scan procedure. The sampling distance was set at 0.1 in. so as to visualize macroscopic errors, such as the Hencky curve and wrinkles, and some microscopic errors that the Ruze equation attempts to characterize.

Data Transformation Routine

Data points obtained from the photogrammetry study are not necessarily in the proper coordinate system that the ideal paraboloid would be known. Therefore, they need to be transformed into the proper coordinate system; that is, one in which the antenna points along the z-axis and the vertex of the antenna is located at the origin of the coordinate system. The focal point of the antenna is to be located in $(0,0,f)$, where the points refer to the Cartesian triplet (x, y, z) and f is the focal length for the paraboloid. The routine for the transformation is performed in Matlab computer software (ref. 7). The algorithm is based on details given in the block diagram of figure 16.

As shown in figure 16, the final step is to compute the rms surface error via methods described in the section Root-Mean-Square Error Calculation. The ideal surface is computed using the known focal length and the measured x- and y-coordinates. The error is computed in the axial direction, which is along the z-axis. The reason for transforming the data points is to be able to properly determine the ideal paraboloid from

$$z = \frac{1}{4f}\left(x^2 + y^2\right) \tag{20}$$

where x,y,z are the Cartesian coordinates along the paraboloid, and f is the focal length of the paraboloid.

Results

This section presents the results of the tests performed on the offset inflatable aperture antenna for six pressurization levels: 0.000, 0.030, 0.040, 0.050, 0.060, and 0.070 in. H_2O. Detailed directivity and beam pattern results from the planar near-field RF scans are provided. Raw and transformed photogrammetry data are presented and are compared with ideal paraboloidal data. The rms surface errors are calculated and, finally, comparisons are made of the surface error loss exhibited in the planar near-field RF scans on the antenna with those predicted from the Ruze equation via the rms surface error.

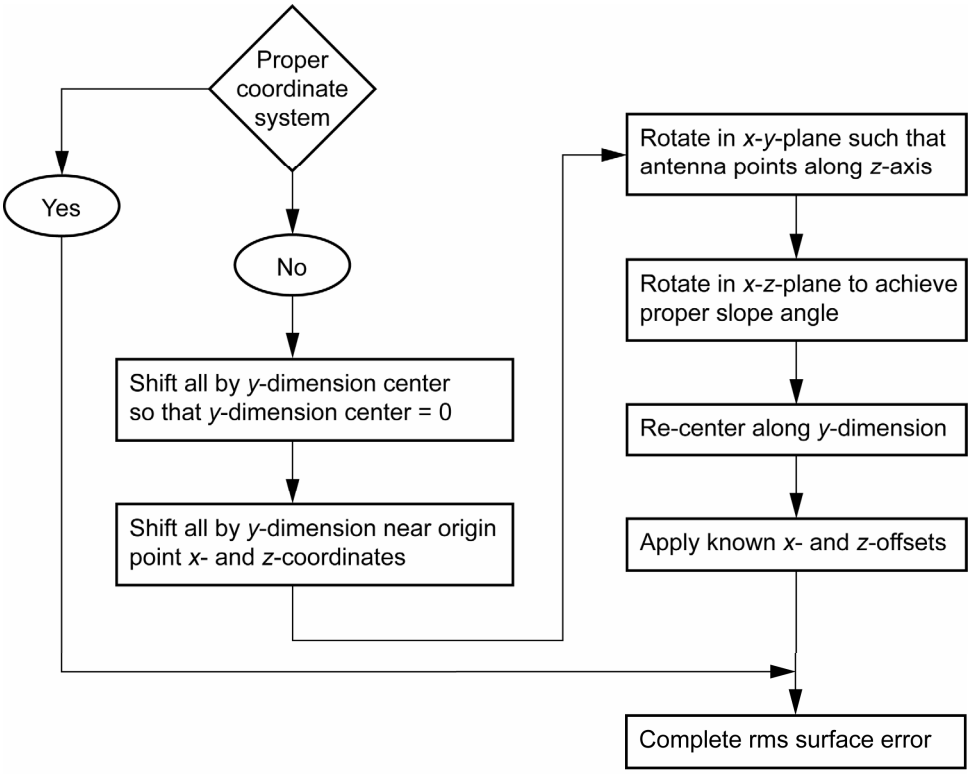

Figure 16.—Coordinate transformation.

Radiofrequency Performance

Planar near-field RF antenna testing results are presented herein. The antenna was tested at 8.4 GHz with a known efficiency of 0.68, based on the loss due to the 11-dB taper from the antenna feed. The ideal antenna gain was 26.753 dBi, based on the diameter of the inflatable aperture antenna and the accounted-for known efficiency. Plots show co-polarization (solid line) and cross-polarization (dashed line) results in the azimuth and elevation dimensions. All graphics were normalized to 0 dBi from the directivity value at that pressurization.

Pressurization level of 0.000 in. H_2O

For this case, an ambient air pressurization of 0.000 in. H_2O meant that the inflatable aperture antenna was uninflated. Because of the effect of gravity, the aperture was not held in the proper direction. The plots of the far-field beam patterns in the azimuth direction are shown in figure 17, and the far-field beam patterns in the elevation direction are shown in figure 18.

The measured directivity of the inflatable aperture antenna was 14.424 dBi. Therefore, the surface loss of the antenna was −12.329 dB. Note that in figure 17, there are no distinguishable nulls present for the co-polarization in the azimuth dimension. In figure 18, there are nulls present at around ±7° with a magnitude that is roughly 7 to 11 dB down below the peak directivity for the co-polarization in the elevation dimension, respectively.

Pressurization level of 0.030 in. H_2O

The antenna was inflated with an ambient air pressure of 0.030 in. H_2O. The plots of the far-field beam patterns in the azimuth direction are shown in figure 19, and the far-field beam patterns in the elevation direction are shown in figure 20.

The measured directivity of the antenna was 23.141 dBi. Therefore, the surface loss of the antenna was −3.612 dB. In figure 19, distinguishable nulls present for the co-polarization at roughly 10° and −12° in the azimuth dimension are roughly 47 and 31 dB down below the peak directivity, respectively. In figure 20, a null is present at around 11° with a magnitude that is roughly 20 dB down below the peak directivity for the co-polarization in the elevation dimension.

Pressurization level of 0.040 in. H_2O

The antenna was inflated with an ambient air pressure of 0.040 in. H_2O. The plots of the far-field beam patterns in the azimuth direction are shown in figure 21, and the far-field beam patterns in the elevation direction are shown in figure 22.

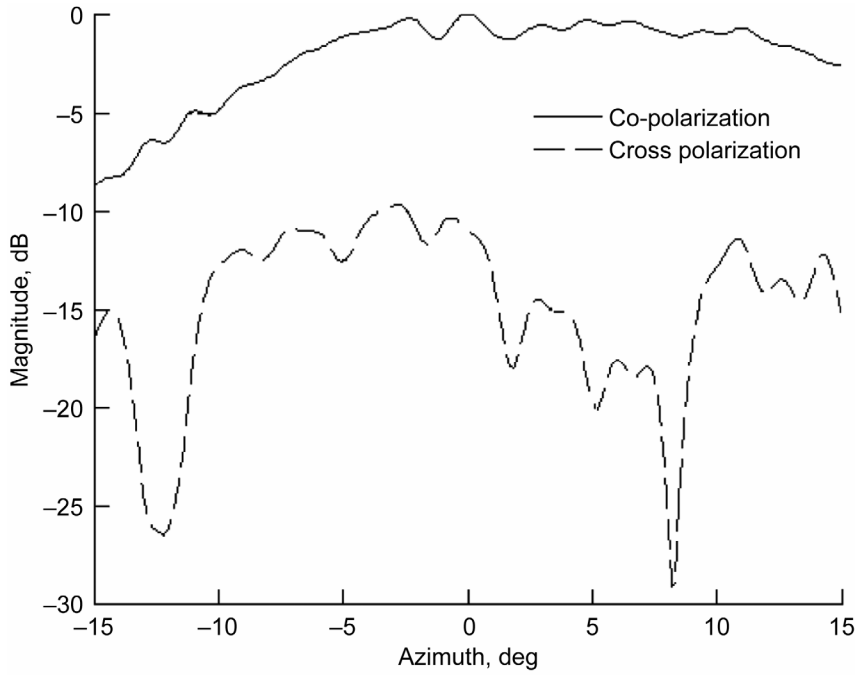

Figure 17.—Azimuth far-field patterns at pressurization of 0.000 in. H_2O.

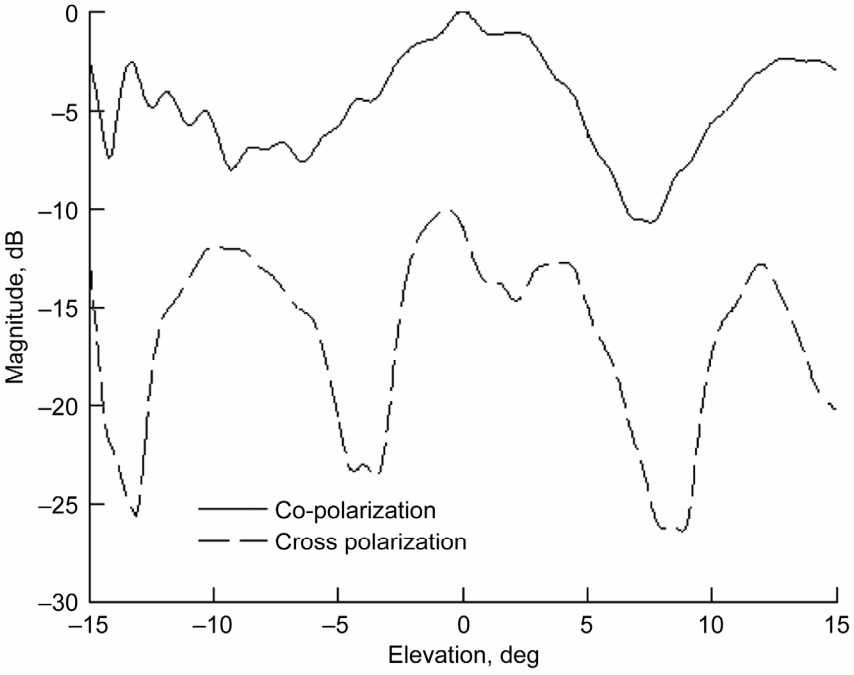

Figure 18.—Elevation far-field patterns at pressurization of 0.000 in. H_2O.

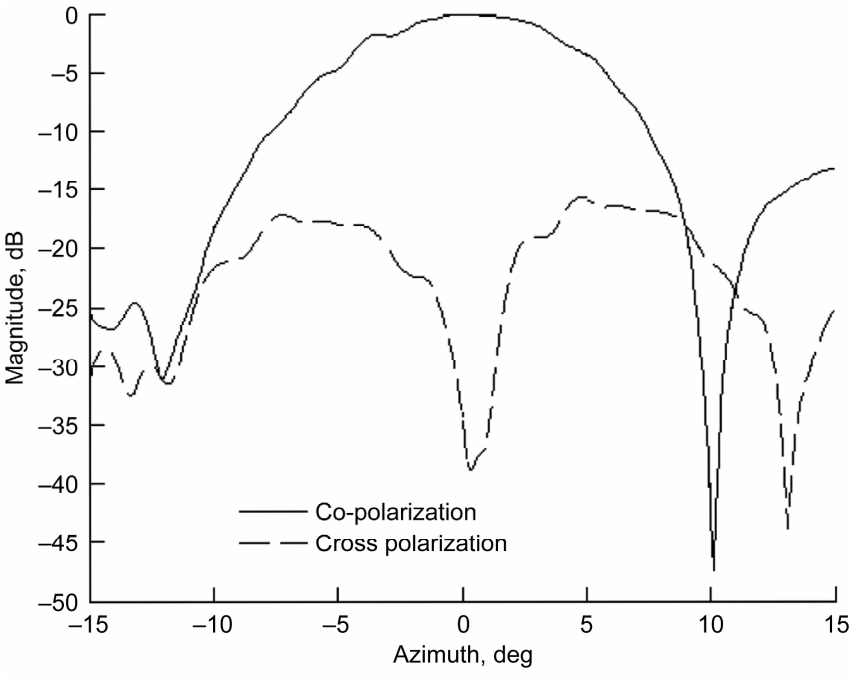

Figure 19.—Azimuth far-field patterns at pressurization of 0.030 in. H_2O.

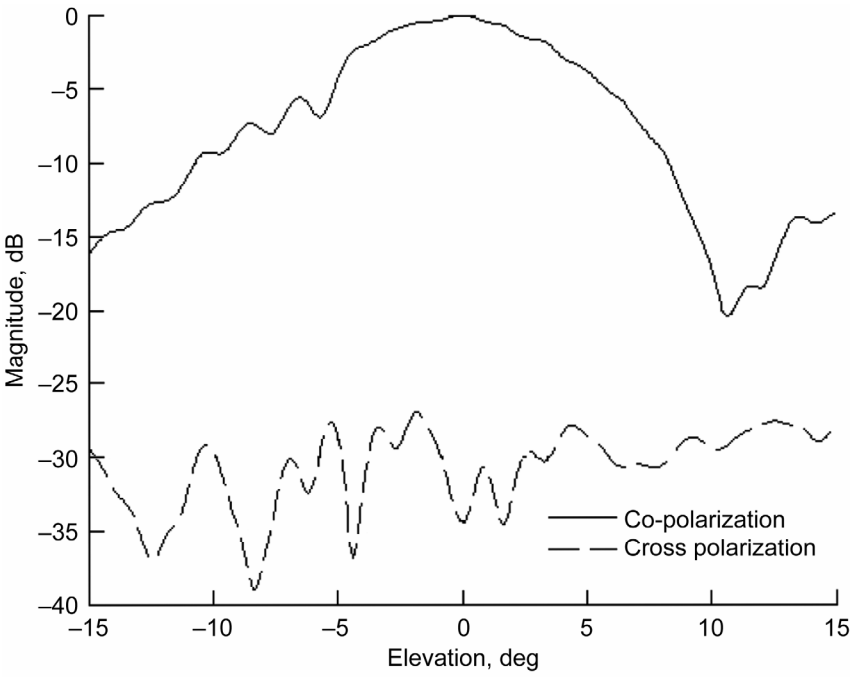

Figure 20.—Elevation far-field patterns at pressurization of 0.030 in. H_2O.

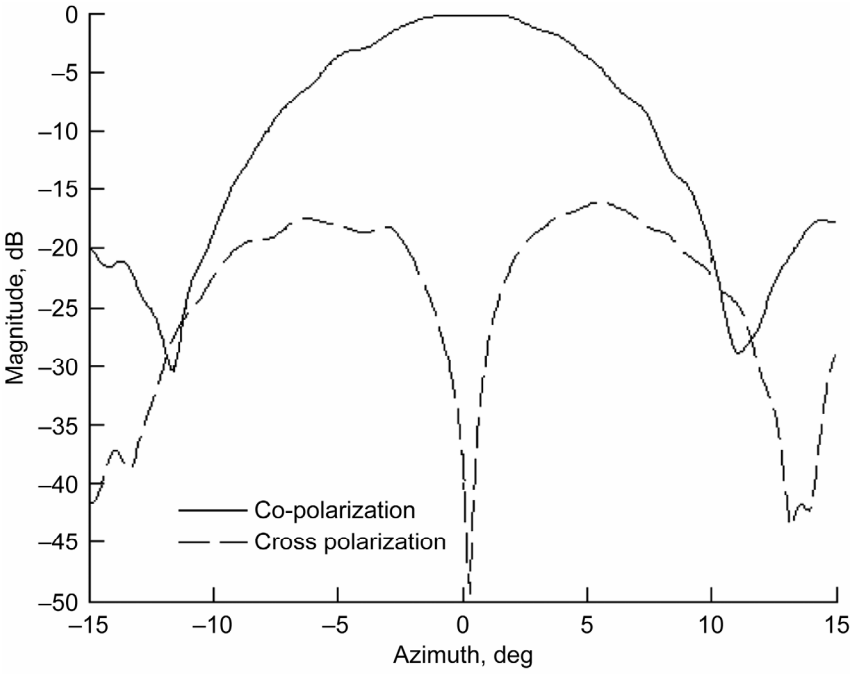

Figure 21.—Azimuth far-field patterns at pressurization of 0.040 in. H_2O.

The measured directivity of the antenna was 24.371 dBi. Therefore, the surface loss of the antenna was −2.382 dB. Note that in figure 21, distinguishable nulls present for the co-polarization at approximately 11° and −11.5° in the azimuth dimension are about 28 and 30 dB down below the peak directivity, respectively. In figure 22, there are nulls present at around 12.5° and −6° with magnitudes that are roughly 18 and 12 dB down below the peak directivity for the co-polarization in the elevation dimension, respectively.

Pressurization level of 0.050 in. H_2O

The antenna was inflated with an ambient air pressure of 0.050 in. H_2O. The plots of the far-field beam patterns in the

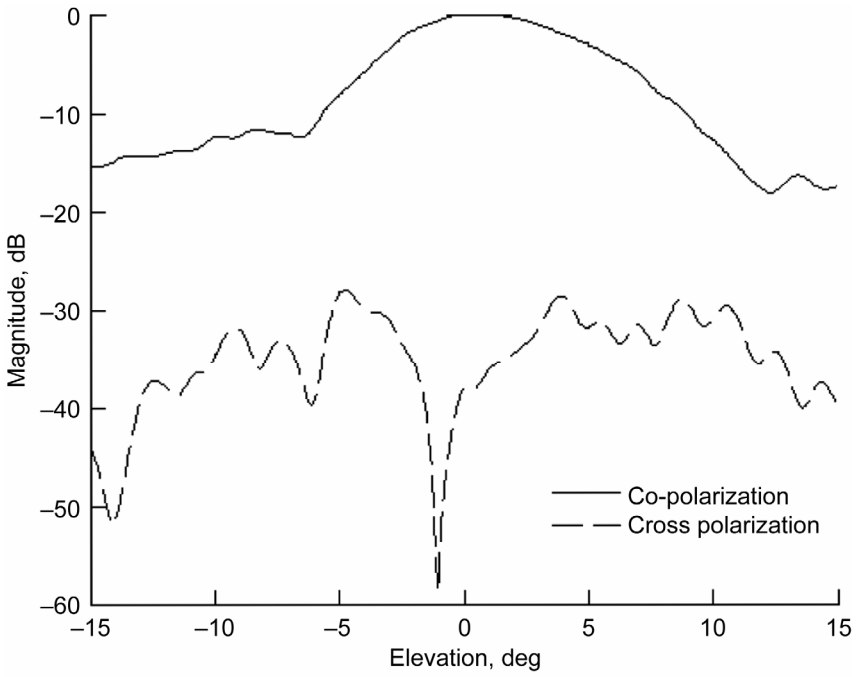

Figure 22.—Elevation far-field patterns at pressurization of 0.040 in. H_2O.

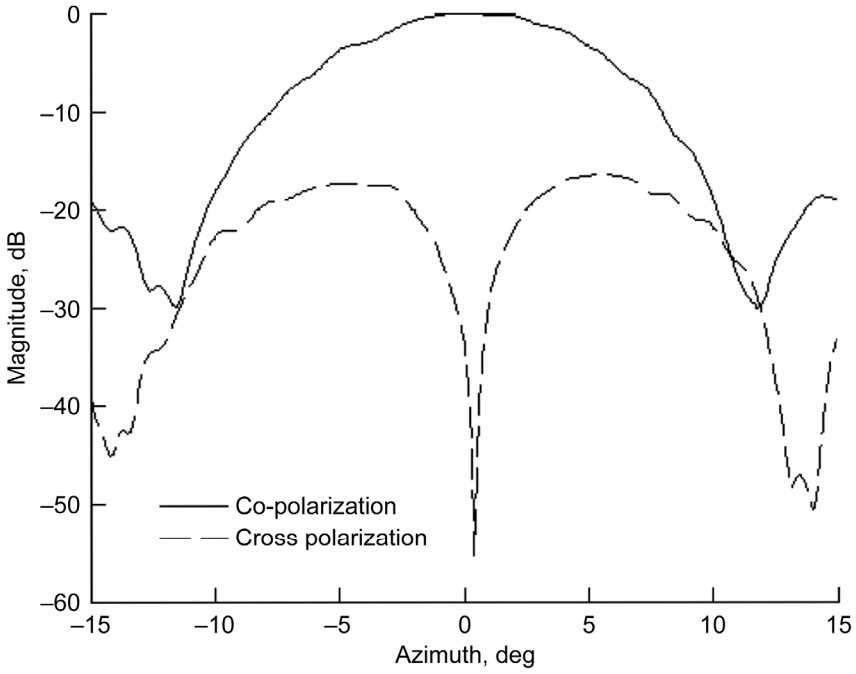

Figure 23.—Azimuth far-field patterns at pressurization of 0.050 in. H_2O.

azimuth direction are shown in figure 23, and the far-field beam patterns in the elevation direction are shown in figure 24.

The measured directivity of the antenna was 24.521 dBi. Therefore, the surface loss of the antenna was −2.232 dB. Note that in figure 23, distinguishable nulls present for the co-polarization at roughly ±12° in the azimuth dimension are approximately 30 dB down below the peak directivity. In figure 24, nulls are present at around 12.5° and −6° with magnitudes that are about 18 and 13 dB down below the peak directivity for the co-polarization in the elevation dimension, respectively.

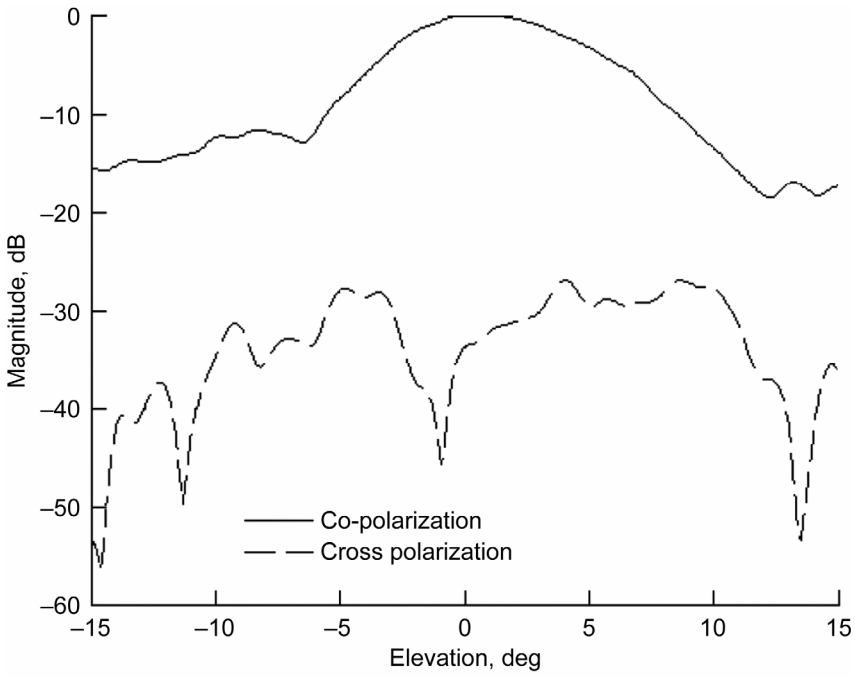

Figure 24.—Elevation far-field patterns at pressurization of 0.050 in. H_2O.

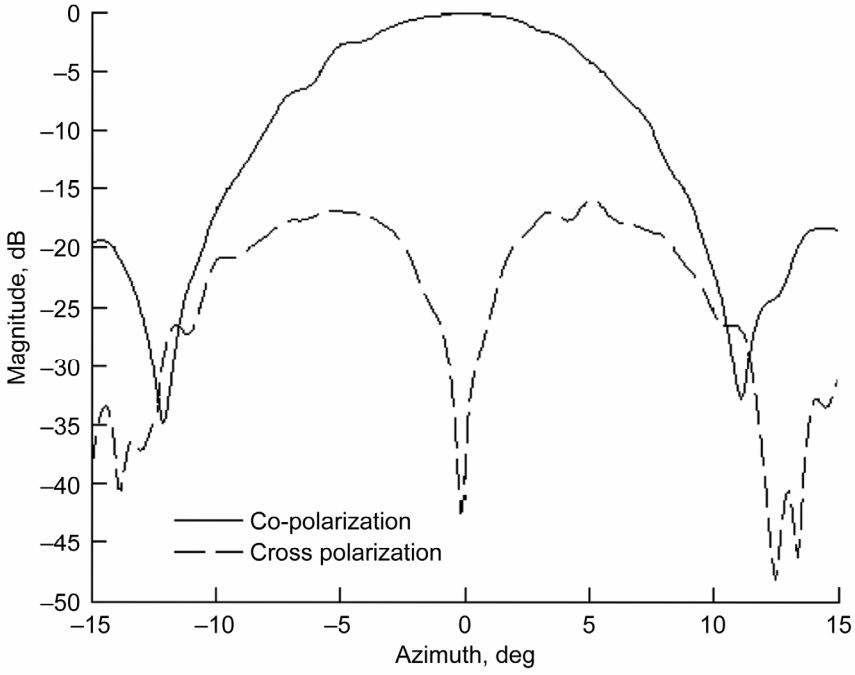

Figure 25.—Azimuth far-field patterns at pressurization of 0.060 in. H_2O.

Pressurization level of 0.060 in. H_2O

The antenna was inflated with an ambient air pressure of 0.060 in. H_2O. The plots of the far-field beam patterns in the azimuth direction are shown in figure 25, and the far-field beam patterns in the elevation direction are shown in figure 26.

The measured directivity of the antenna was 24.473 dBi. Therefore, the surface loss of the antenna was −2.280 dB. Note that in figure 25, distinguishable nulls present for the co-polarization at about 11.5° and −12° in the azimuth dimension are approximately 33 and 35 dB down below the peak directivity, respectively. In figure 26, there are nulls present at around 12.5° and −6° with magnitudes that are roughly 19 and 13 dB down below the peak directivity for the co-polarization in the elevation dimension, respectively.

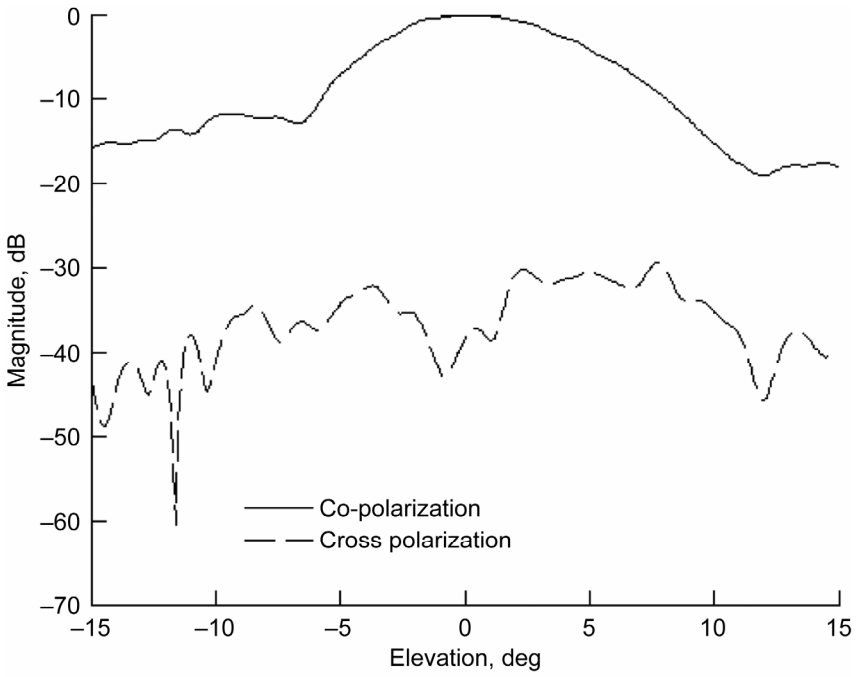

Figure 26.—Elevation far-field patterns at pressurization of 0.060 in. H_2O.

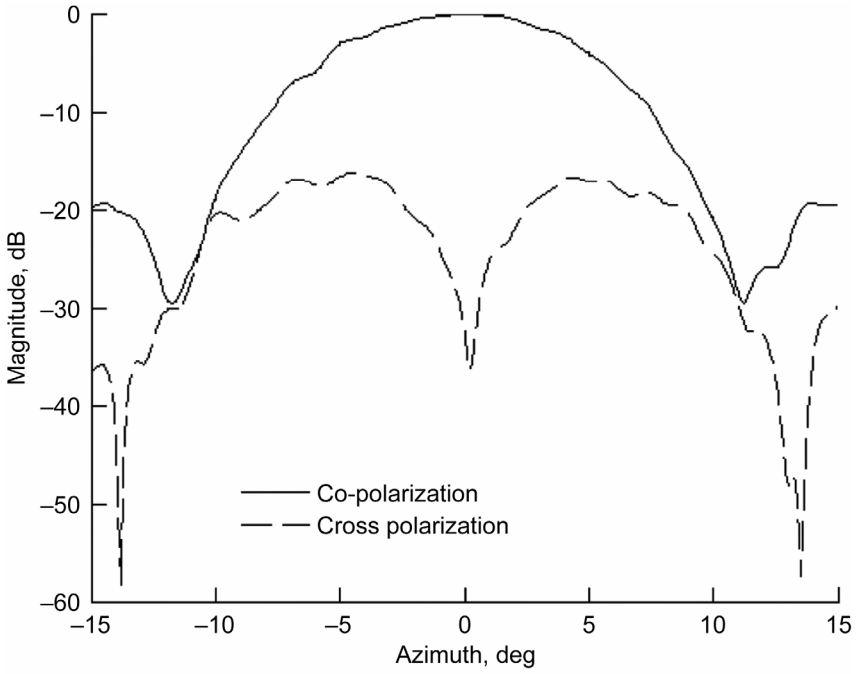

Figure 27.—Azimuth far-field patterns at pressurization of 0.070 in. H_2O.

Pressurization level of 0.070 in. H_2O

The antenna was inflated with an ambient air pressure of 0.070 in. H_2O. The plots of the far-field beam patterns in the azimuth direction are shown in figure 27, and the far-field beam patterns in the elevation direction are shown in figure 28.

The measured directivity of the antenna was 24.453 dBi. Therefore, the surface loss of the antenna was −2.300 dB. Note that in figure 27, distinguishable nulls present for the co-polarization at roughly 11.5° and −12° in the azimuth dimension are about 30 dB down below the peak directivity. In figure 28, there are nulls present at around 12° and −6.5°

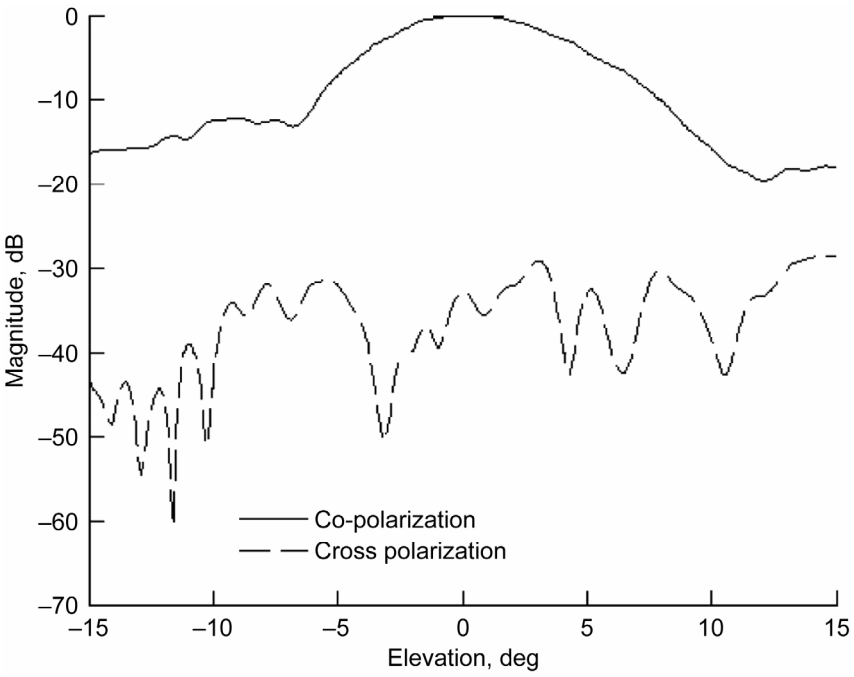

Figure 28.—Elevation far-field patterns at pressurization of 0.070 in. H_2O.

with magnitudes that are approximately 20 and 13 dB down below the peak directivity for the co-polarization in the elevation dimension, respectively.

Radiofrequency performance summary

Table III presents a summary of the directivity and the surface loss experienced by the 0.3-m offset antenna for the six pressurizations at which the antenna was tested. Note that the pressurization that produced the largest directivity was 0.050 in. H_2O.

TABLE III.—COMPARISON OF RADIOFREQUENCY PRESSURIZATION PERFORMANCE

Pressurization, in. H_2O	Radio frequency directivity, dBi	Surface loss, dB
0.000	14.424	−12.329
.030	23.141	−3.612
.040	24.371	−2.382
.050	24.521	−2.232
.060	24.473	−2.280
.070	24.453	−2.300

Root-Mean-Square Performance

Photogrammetry antenna testing results are presented herein. The antenna was scanned at spacing intervals of 0.1 in. in the *x*- and *y*-dimensions This spatial separation between intervals is well below the Nyquist minimum of 0.703 in. Presented are plots of both the raw photogrammetry data and the transformed photogrammetry data with the ideal paraboloid shown in the *x*-*z* plane, in which the transformed data are darker than the ideal paraboloid.

Pressurization level of 0.000 in. H_2O

The antenna was inflated with an ambient air pressure of 0.000 in. H_2O, meaning that for this case the antenna was uninflated. Because of the effect of gravity, the aperture was not held in the proper direction. The raw photogrammetry data are shown in figure 29, and the transformed photogrammetry data and the ideal paraboloid are shown in figure 30.

The calculated rms surface error was 1.2036 in. Therefore, according to the Ruze equation, the surface loss should be –402.015 dB. Figure 29 shows clearly defined wrinkles on the antenna surface. Figure 30 reveals that the antenna is no longer maintaining its shape as gravity has caused it to become inverted. Note also that the Hencky curve can still be observed near the antenna edges.

Pressurization level of 0.030 in. H_2O

The antenna was inflated with an ambient air pressure of 0.030 in. H_2O. The raw photogrammetry data are shown in figure 31, and the transformed photogrammetry data and the ideal paraboloid are shown in figure 32.

The calculated rms surface error was 0.3407 in. Therefore, according to the Ruze equation, the surface loss should be –32.212 dB. Figure 31 shows one large wrinkle and several smaller wrinkles on the antenna surface. Figure 32 shows how the antenna was affected by the inflation process in that the Hencky curve was created near the antenna edges.

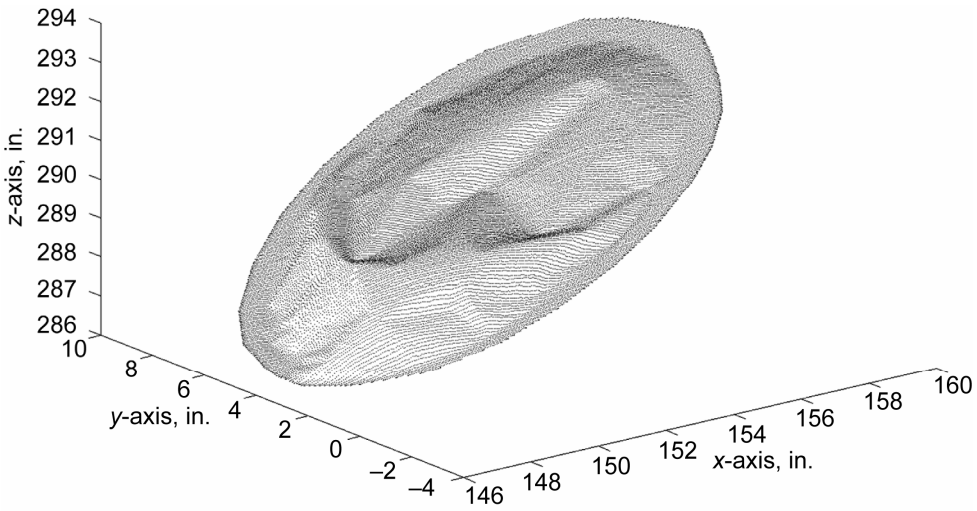

Figure 29.—Raw photogrammetry data at pressurization of 0.000 in. H_2O.

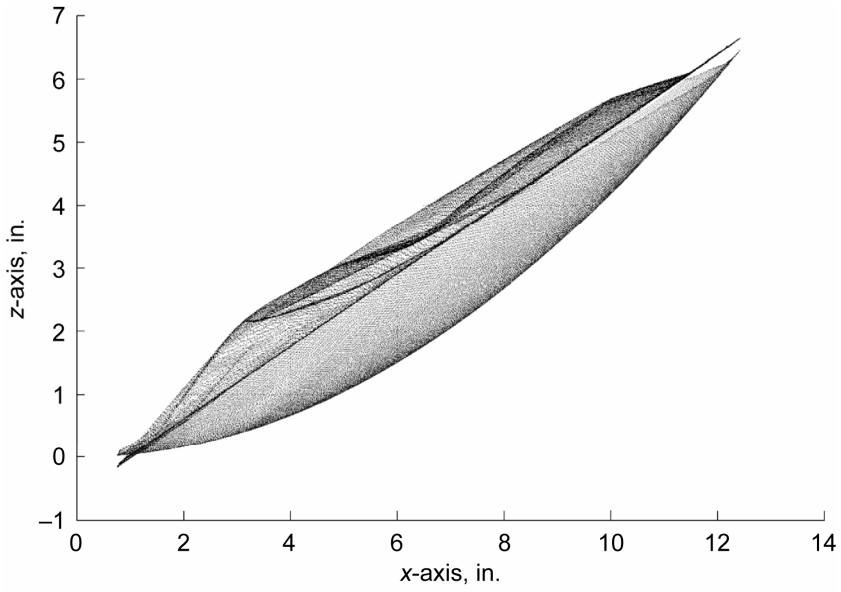

Figure 30.—Transformed and ideal paraboloid at pressurization of 0.000 in. H_2O.

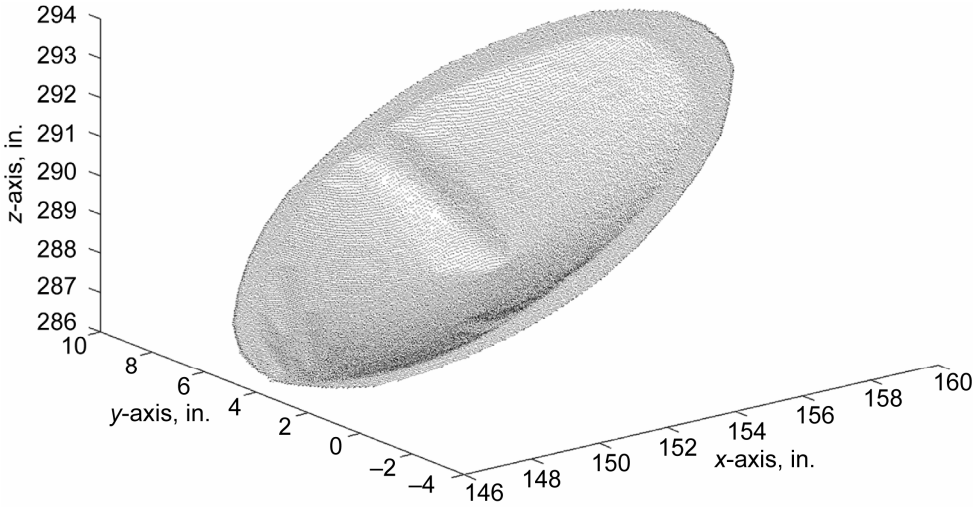

Figure 31.—Raw photogrammetry data at pressurization of 0.030 in. H_2O.

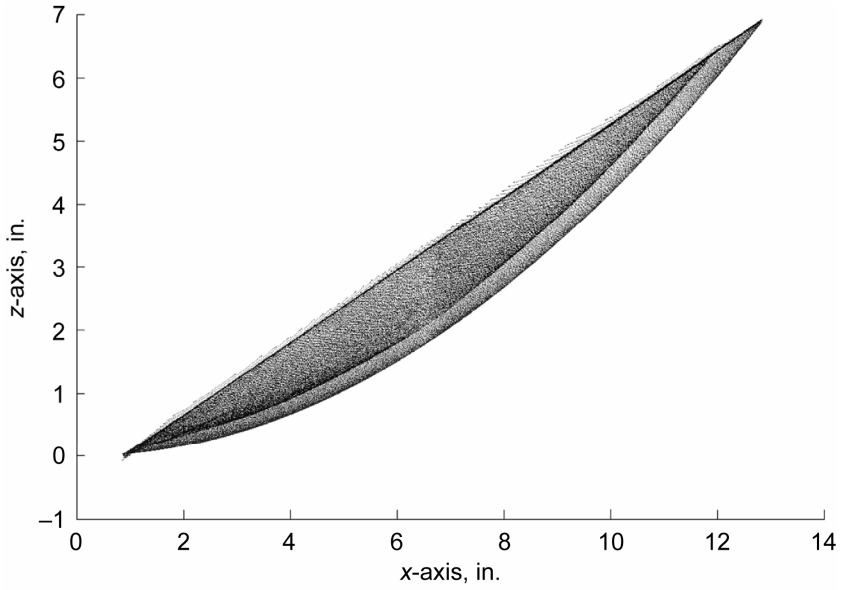

Figure 32.—Transformed and ideal paraboloid at pressurization of 0.030 in. H_2O.

Pressurization level of 0.040 in. H_2O

The antenna was inflated with an ambient air pressure of 0.040 in. H_2O. The raw photogrammetry data are shown in figure 33, and the transformed photogrammetry data and the ideal paraboloid are shown in figure 34.

The calculated rms surface error was 0.2620 in. Therefore, according to the Ruze equation, the surface loss should be –19.049 dB. Figure 33 shows that several more smaller wrinkles existed on the antenna surface than existed at lower pressurizations. Figure 34 shows how the antenna was affected by the inflation process, in that the Hencky curve was created near the antenna edges. Note that as the pressurization increases, the amount of the antenna surface affected by the Hencky curve decreases.

Pressurization level of 0.050 in. H_2O

The antenna was inflated with an ambient air pressure of 0.050 in. H_2O. The raw photogrammetry data are shown in figure 35, and the transformed photogrammetry data and the ideal paraboloid are shown in figure 36.

The calculated rms surface error was 0.2334 in. Therefore, according to the Ruze equation, the surface loss should be –15.117 dB. Figure 35 shows that several smaller wrinkles existed on the antenna surface than existed at lower pressurizations. Figure 36 shows how the antenna was affected by the inflation process, in that the Hencky curve was created near the antenna edges. Note that as the pressurization increases, the amount of the antenna surface affected by the Hencky curve decreases.

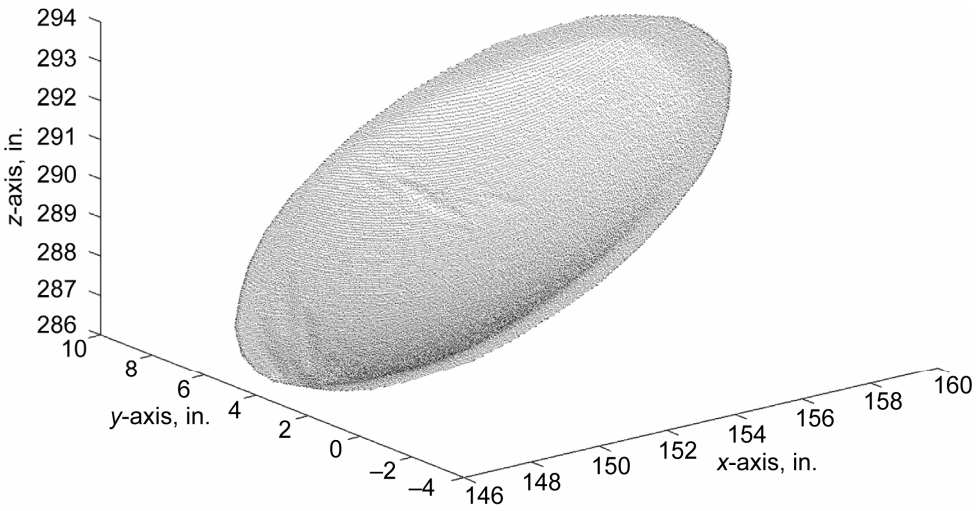

Figure 33.—Raw photogrammetry data at pressurization of 0.040 in. H_2O.

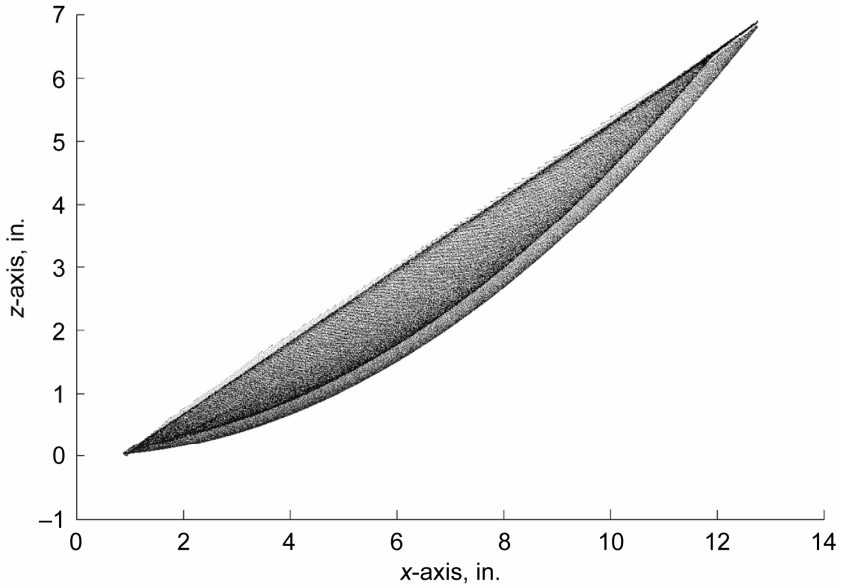

Figure 34.—Transformed and ideal paraboloid at pressurization of 0.040 in. H_2O.

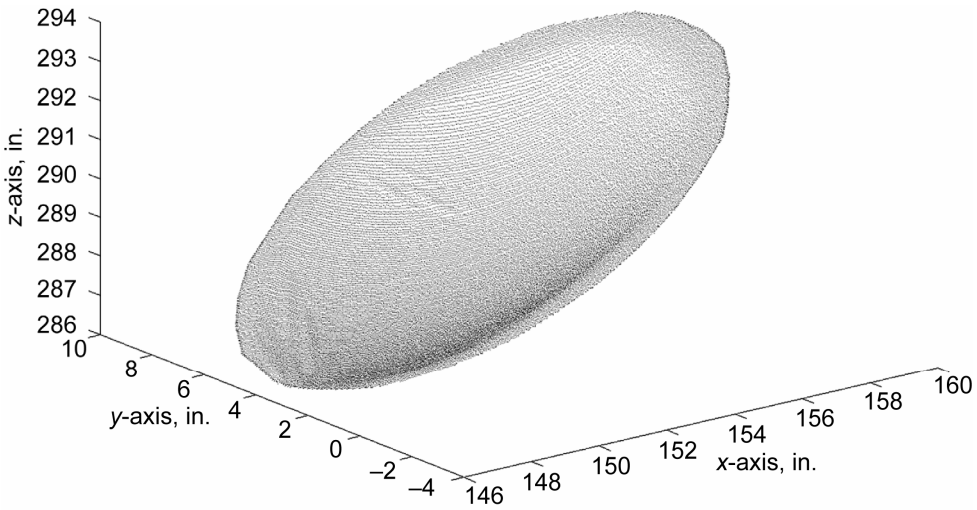

Figure 35.—Raw photogrammetry data at pressurization of 0.050 in. H_2O.

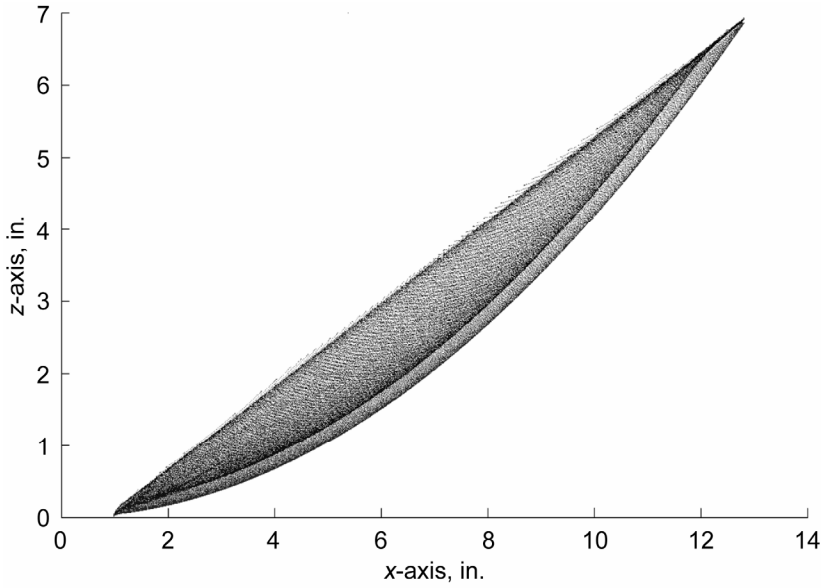

Figure 36.—Transformed and ideal paraboloid at pressurization of 0.050 in. H_2O.

Pressurization level of 0.060 in. H_2O

The antenna was inflated with an ambient air pressure of 0.060 in. H_2O. The raw photogrammetry data are shown in figure 37, and the transformed photogrammetry data and the ideal paraboloid are shown in figure 38.

The calculated rms surface error was 0.1885 in. Therefore, according to the Ruze equation, the surface loss should be –9.861 dB. Figure 37 shows a few very small wrinkles on the antenna surface near the region of inflation control for the aperture. Figure 38 shows how the antenna was affected by the inflation process, in that the Hencky curve was created near the antenna edges. Note that at this pressurization, there was less an effect from the Hencky curve than there was at prior pressurizations.

Pressurization level of 0.070 in. H_2O

The antenna was inflated with an ambient air pressure of 0.070 in. H_2O. The raw photogrammetry data are shown in figure 39, and the transformed photogrammetry data and the ideal paraboloid are shown in figure 40.

The calculated rms surface error was 0.2649 in. Therefore, according to the Ruze equation, the surface loss should be –19.473 dB. Figure 39 shows a few very small wrinkles on the antenna surface near the region of inflation control for the aperture. Figure 40 shows how the antenna was affected by the inflation process, in that the Hencky curve was created near the antenna edges. Note that at this pressurization, the antenna is starting to become overinflated as can be seen in the comparison of the ideal and measured paraboloids.

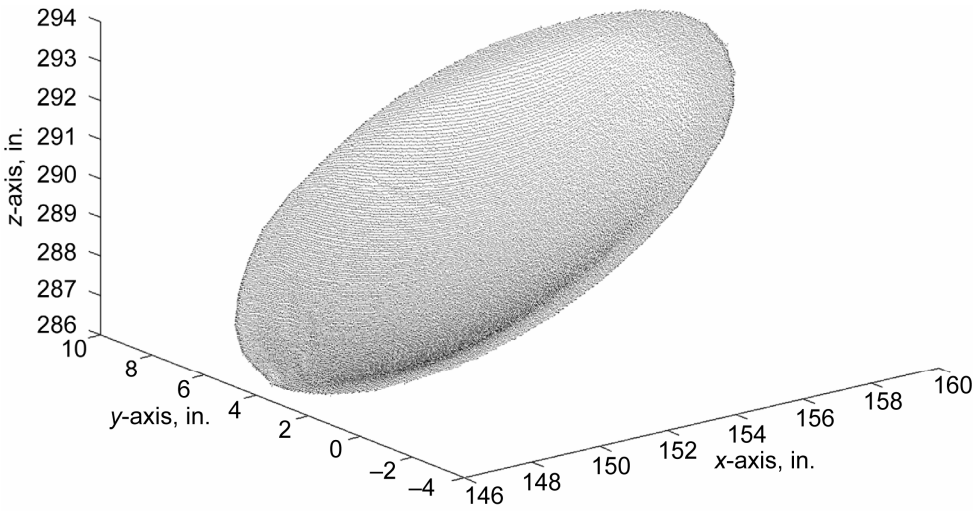

Figure 37.—Raw photogrammetry data at pressurization of 0.060 in. H_2O.

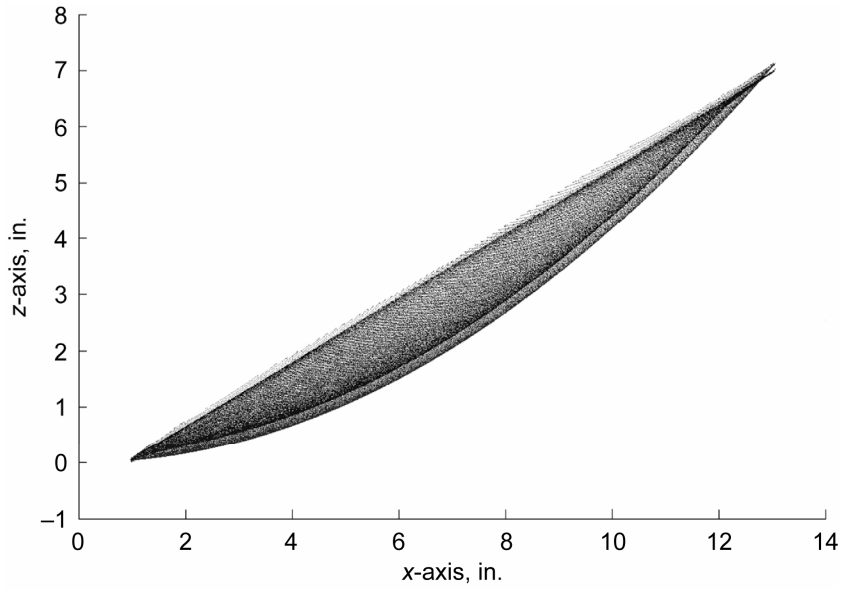

Figure 38.—Transformed and ideal paraboloid at pressurization of 0.060 in. H_2O.

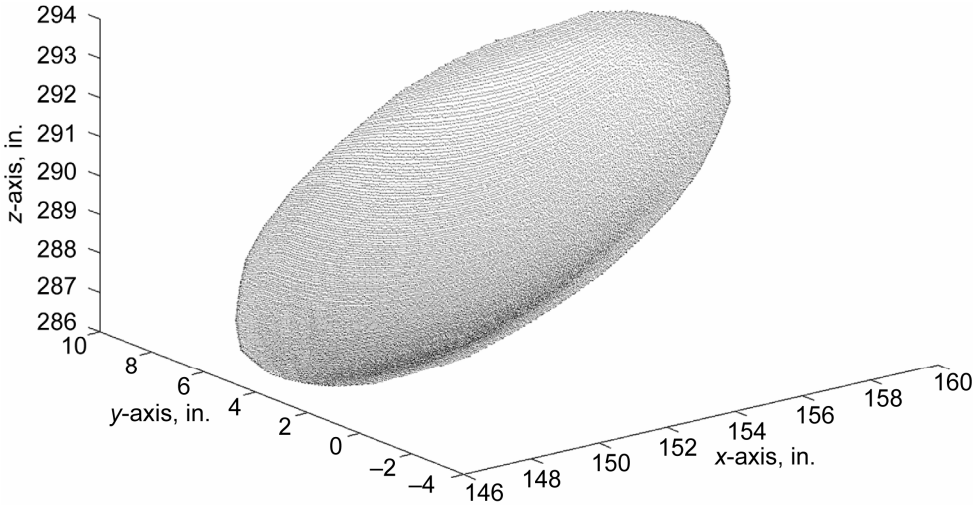

Figure 39.—Raw photogrammetry data at pressurization of 0.070 in. H_2O.

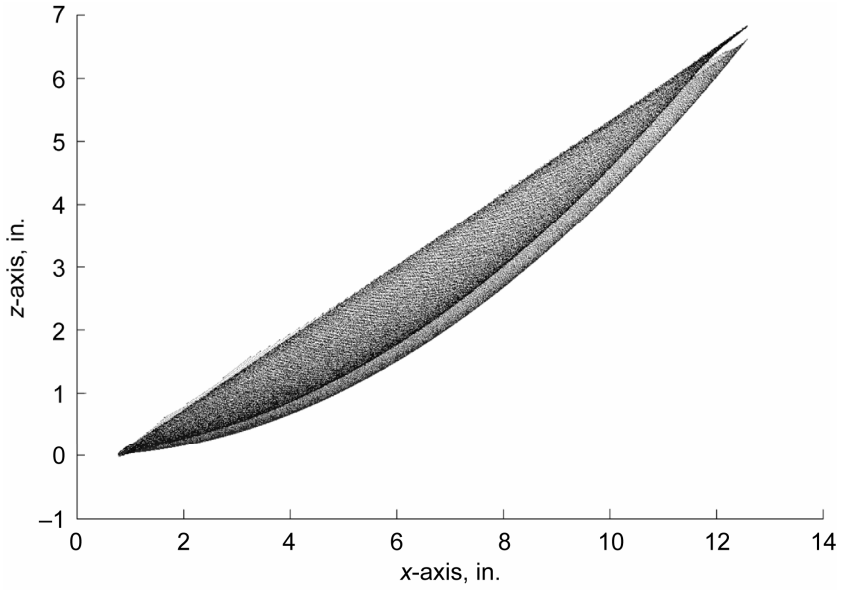

Figure 40.—Transformed and ideal paraboloid at pressurization of 0.070 in. H_2O.

Root-mean-square performance summary

Table IV summarizes the rms surface error and the Ruze equation predicted surface loss for the 0.3-m offset antenna for the six pressurizations at which the antenna was tested. Note that the pressurization that produced the smallest rms surface error was 0.060 in. H_2O. This is not the same pressurization that produced the largest directivity from the RF pressurization performance analysis.

TABLE IV.—COMPARISON OF ROOT-MEAN-SQUARE PRESSURIZATION PERFORMANCE

Pressurization, in. H_2O	Root-mean-square surface error, in.	Ruze-derived surface loss, dB
0.000	1.2036	−402.015
.030	.3407	−32.212
.040	.2620	−19.049
.050	.2334	−15.117
.060	.1885	−9.861
.070	.2649	−19.473

Ruze Equation Performance

The two previous sections provided information about the directivity and beam pattern measurements taken from the planar near-field antenna test facility at NASA Glenn Research Center and the photogrammetry-derived Ruze equation predictions for the directivity degradation due to surface errors. These results are presented in table V for the six pressurization levels. The difference between the RF performance and the Ruze-derived performance is also calculated. Note that a positive number means that the Ruze equation overstates the surface loss.

Several notable facts become evident from table V. First, the pressurization with the largest directivity of 24.521 dBi was at 0.050 in. H_2O. At this pressurization, the surface loss experienced was −2.232 dB and the rms surface error was 0.2334 in., which correlates with a Ruze directivity degradation of −15.117 dB. This result means that the Ruze equation overstates the directivity degradation by 12.885 dB.

However, the pressurization with the smallest rms surface error was at 0.060 in. H_2O with an rms surface error of 0.1885 in. This rms surface error, according to Ruze, produces a directivity degradation of −9.861 dB. The RF performance at this pressurization level was 24.473 dB, producing a surface loss of −2.280 dB. This result indicates that the Ruze equation overstates the directivity degradation by 7.580 dB.

For all six pressurization levels, the Ruze equation overstates the degradation in the directivity. The lowest overstatement of the degradation in directivity was 7.580 dB at a pressurization of 0.060 in. H_2O. The largest overstatement of the degradation in the directivity was 389.686 dB at a pressurization of 0.000 in. H_2O (while the antenna was not inflated).

Finally, it is important to note that the Ruze equation does not provide any information on the beam patterns that characterize the antenna. As shown in figures 17 through 28, the first nulls off the main beam occur at slightly different locations based on the pressurization level. Also, these nulls each have different amplitudes. For full characterization of the antenna performance, utilizing the Ruze equation for the directivity degradation provides zero information on the nature of the beam patterns that define the performance of the antenna.

Conclusions

Testing was conducted on a 0.3-m offset inflatable aperture antenna at 8.4 GHz at six different pressurization levels: 0.000, 0.030, 0.040, 0.050, 0.060, and 0.070 in. H_2O. The Ruze equation was used to estimate the surface loss of the antenna. The equation utilizes the root-mean-square (rms) surface error that is calculated from photogrammetry data to compute a directivity degradation value. However, it was shown that the surface loss which the Ruze equation predicts was not accurate for the membrane aperture antennas of interest here. For the offset inflatable aperture antenna tested in this study, the Ruze equation overstated the directivity degradation. At the lowest rms surface error produced from the multiple pressurization levels at which the offset inflatable aperture antenna was tested, the Ruze equation overstated the surface loss by 7.58 dB. However, for the worst case when the antenna was not inflated and inverted, the Ruze equation overstated the surface loss by about 390 dB.

It is believed that the reason the Ruze equation overstates the surface loss is due to the types of errors that the inflatable aperture antennas need to overcome. The Ruze equation assumes that the errors are random in nature, are uniformly distributed over the aperture, are distributed in fixed, circular correlation regions with a diameter that is much smaller than the diameter of the antenna, and have a Gaussian spatial phase correlation. However, inflatable aperture antennas suffer from surface errors involving wrinkles due to underinflation and from the Hencky curve created near the antenna edges. Neither of these errors is random on the antenna surface. Wrinkles occur along locations of the antenna where the pressurization does not create enough strain on the inflatable membrane material. Hencky-type errors always occur near the edge of the antenna. Thus, Hencky-type errors are not uniform over the antenna aperture. Typically, wrinkles will be present along the entire aperture if the antenna is properly inflated. Neither wrinkles nor Hencky curve errors occur in fixed, circular correlation regions. Wrinkles can take on an elliptical shape, whereas Hencky errors will surround the entire antenna. Therefore, the correlation regions, regardless of shape, are not much smaller than the diameter of the antenna.

TABLE V.—COMPARISONS OF RADIOFREQUENCY AND RUZE EQUATION PERFORMANCE

Pressurization, in. H_2O	Radiofrequency directivity, dBi	Radiofrequency-derived surface loss, dB	Root-mean-square surface error, in.	Ruze-derived surface loss, dB	Difference,[a] dB
0.000	14.424	−12.329	1.2036	−402.015	389.686
.030	23.141	−3.612	.3407	−32.212	28.600
.040	24.371	−2.382	.2620	−19.049	16.667
.050	24.521	−2.232	.2334	−15.117	12.885
.060	24.473	−2.280	.1885	−9.861	7.580
.070	24.453	−2.300	.2649	−19.473	17.173

[a]Positive number indicates that Ruze equation overstates surface loss.

The dominant errors that are associated with inflatable aperture antennas do not correspond to those associated with the types of errors that the Ruze equation takes into account.

The Ruze equation is also limited in what it can predict. Although the Ruze equation attempts to characterize the surface loss, it makes no predictions of the characteristics of the secondary beam patterns. Typically, it is important to understand the locations of the first nulls off the main beam, in addition to how far down below the directivity those nulls are. Side lobes are also not accounted for in the Ruze equation, whether it is the peak location or the amplitude. These antenna beam pattern characteristics are important and must be fully understood prior to operation of the antenna.

In conclusion, it is recommended that the Ruze equation not be used to predict antenna performance for inflatable aperture antennas. The application of the Ruze equation to estimate the surface loss was not effective because it overstated the surface loss experienced by inflatable aperture antennas and did not provide any information about the beam patterns.

Future Work

The current study analyzed the problem of understanding and replicating in computer-based simulations the amount of degradation there will be in directivity for inflatable antennas. Future work on this problem involves several areas. First, the immediate follow-on effort will be to utilize the photogrammetry data points to propagate the far-field beam patterns and directivity. The methodology will be to utilize the theory of geometrical optics and edge-diffracted fields to obtain the near-field amplitude and phase plots. Fourier transform techniques will then transform the near-field data into the far-field data, from which the beam patterns and directivity can be calculated. One necessary step is to create a method to compute the direction of the reflected rays from the antenna surface. Since the antenna will not be known from a continuous function, there is not an equation from which derivatives can be computed to determine the surface normal vector. Instead, the data points surrounding the surface point in question will be utilized to determine the local tangent and normal vector to the surface point. After the normal vector is computed, Snell's law will be utilized to determine the vector direction that the reflected ray will travel. This software code will also be extended beyond the use for offset inflatable aperture antennas to others such as the inflatable Cassegrain aperture antennas.

After the software code is functional, plans are in place to perform dynamic photogrammetry studies of the 1-m class inflatable antenna inside a thermal vacuum chamber. Targeted or projection photogrammetry of the antenna surface will likely be performed. Alternatively, laser scanning may be performed through windows located on the walls of the chamber by using stationary mirrors located inside the thermal vacuum chamber. A second proposed study is to examine the effects of gravity over time as they relate to the sag on the antenna. Since the shape of the inflatable antenna is not constant over time (resulting from inflation pressurization changes), gravity can deform the actual shape from the ideal paraboloid. The study will examine the effects of gravity over time with constant inflation pressurization to understand how the paraboloidal shape deforms. To understand how the antenna may perform in space after inflation, the goal will be to try to back out all the effects of gravity, starting from before the first instance that gravity has deformed the shape.

The final proposed study is to create an equation that will account for all the types of errors associated with inflatable aperture antennas, such as random microscopic surface errors, such as those that the Ruze equation can deal with, and deterministic macroscopic surface errors associated with the Hencky curve, wrinkles, and overinflation. The equation could provide a means for accurately approximating the directivity degradation for inflatable aperture antennas.

References

1. Ruze, John: Antenna Tolerance Theory—A Review. Proceedings of the IEEE, vol. 54, no. 4, 1966, pp. 633–640.
2. Balanis, Constantine A.: Antenna Theory: Analysis and Design. John Wiley & Sons, New York, NY, 1982.
3. Bao, X.Q., et al.: Wirelessly Controllable Inflated Electroactive Polymer (EAP) Reflectors. Proc. Soc. Photo Opt. Instrum. Eng., vol. 5759, 2005, pp. 371–378.
4. Williams, W.: High Capacity Communications From Martian Distances. NASA/TM—2006–214415, 2007.
5. Gaspar, James L., et al.: Test and Analysis of an Inflatable Parabolic Dish Antenna. AIAA–2006–1600, 2006.
6. Pearson, James C., Jr.: Phase III Inflatable Membrane Antennas. NASA TR04–1052, 2004. Available from the NASA Center for Aerospace Information.
7. Pearson, J.; and Romanofsky, R.: Thin Film Antenna Development and Optimization. AIAA–2006–2229, 2006.
8. Romanofsky, Robert R.: The Potential for Gossamer Deployable Antenna Systems in Ka-Band Exploration and Science Communications Architectures. Presented at the 12th Ka-Band and Broadband Communications Conference, Naples, Italy, Sept. 2006.
9. Hoferer, Robert A.; and Rahmat-Samii, Yahya: RF Characterization of an Inflatable Parabolic Torus Reflector Antenna for Space-Borne Applications. IEEE Trans. Antennas Propag., vol. 46, issue 10, 1998, pp. 1449–1457.
10. Jenkins, C.H., et al.: Intelligent Shape Control for Precision Membrane Antennae and Reflectors in Space. Smart Material Structures, vol. 8, no. 6, 1999, pp. 857–867.
11. Zocchi, F.E.: Estimation of the Accuracy of a Reflector Surface From the Measured rms Error. IEEE Trans. Instrum. Meas., vol. 54, issue 5, 2005, pp. 2124–2129.
12. Acosta, R.J.; and Lee, R.Q.: Case Study of Sample Spacing in Planar Near-Field Measurement of High Gain Antennas. NASA TM–86872, 1984.

Glenn Research Center
National Aeronautics and Space Administration
Cleveland, Ohio, April 21, 2008

REPORT DOCUMENTATION PAGE		Form Approved OMB No. 0704-0188

1. REPORT DATE *(DD-MM-YYYY)*	2. REPORT TYPE	3. DATES COVERED *(From - To)*
01-04-2008	Technical Paper	

4. TITLE AND SUBTITLE
Application of Ruze Equation for Inflatable Aperture Antennas

5a. CONTRACT NUMBER

5b. GRANT NUMBER

5c. PROGRAM ELEMENT NUMBER

6. AUTHOR(S)
Welch, Bryan, W.

5d. PROJECT NUMBER

5e. TASK NUMBER

5f. WORK UNIT NUMBER
WBS 439432.04.04.01

7. PERFORMING ORGANIZATION NAME(S) AND ADDRESS(ES)
National Aeronautics and Space Administration
John H. Glenn Research Center at Lewis Field
Cleveland, Ohio 44135-3191

8. PERFORMING ORGANIZATION REPORT NUMBER
E-16182

9. SPONSORING/MONITORING AGENCY NAME(S) AND ADDRESS(ES)
National Aeronautics and Space Administration
Washington, DC 20546-0001

10. SPONSORING/MONITORS ACRONYM(S)
NASA

11. SPONSORING/MONITORING REPORT NUMBER
NASA/TP-2008-214953

12. DISTRIBUTION/AVAILABILITY STATEMENT
Unclassified-Unlimited
Subject Category: 32
Available electronically at http://gltrs.grc.nasa.gov
This publication is available from the NASA Center for AeroSpace Information, 301-621-0390

13. SUPPLEMENTARY NOTES

14. ABSTRACT
Inflatable aperture reflector antennas are an emerging technology that NASA is investigating for potential uses in science and exploration missions. As inflatable aperture antennas have not been proven fully qualified for space missions, they must be characterized properly so that the behavior of the antennas can be known in advance. To properly characterize the inflatable aperture antenna, testing must be performed in a relevant environment, such as a vacuum chamber. Since the capability of having a radiofrequency (RF) test facility inside a vacuum chamber did not exist at NASA Glenn Research Center, a different methodology had to be utilized. The proposal to test an inflatable aperture antenna in a vacuum chamber entailed performing a photogrammetry study of the antenna surface by using laser ranging measurements. A root-mean-square (rms) error term was derived from the photogrammetry study to calculate the antenna surface loss as described by the Ruze equation. However, initial testing showed that problems existed in using the Ruze equation to calculate the loss due to errors on the antenna surface. This study utilized RF measurements obtained in a near-field antenna range and photogrammetry data taken from a laser range scanner to compare the expected performance of the test antenna (via the Ruze equation) with the actual RF patterns and directivity measurements. Results showed that the Ruze equation overstated the degradation in the directivity calculation. Therefore, when the photogrammetry study is performed on the test antennas in the vacuum chamber, a more complex equation must be used in light of the fact that the Ruze theory overstates the loss in directivity for inflatable aperture reflector antennas.

15. SUBJECT TERMS
Reflector antenna; Inflatable structure; Large deployable reflector; Surface distortion; Phase error; Antenna

16. SECURITY CLASSIFICATION OF:			17. LIMITATION OF ABSTRACT	18. NUMBER OF PAGES	19a. NAME OF RESPONSIBLE PERSON
a. REPORT	b. ABSTRACT	c. THIS PAGE			STI Help Desk (email:help@sti.nasa.gov)
U	U	U	UU	35	19b. TELEPHONE NUMBER *(include area code)* 301-621-0390